MECHANICAL SIGNALING INDUCED CELLULAR REMODELING STUDIED BY INTEGRATED OPTICAL AND ATOMIC FORCE MICROSCOPY

A Dissertation

by

HARINI BYTARAYA SREENIVASAPPA

Submitted to the Office of Graduate and Professional Studies of
Texas A&M University
in partial fulfillment of the requirements for the degree of

DOCTOR OF PHILOSOPHY

Chair of Committee	Andreea Trache
Committee Members	Wonmuk Hwang
	Alvin Yeh
	Robert Burghardt
Head of Department	Gerard Coté

December 2014

Major Subject: Biomedical Engineering

ABSTRACT

Vascular wall composition and mechanics are important for cardiovascular physiology and pathology. The reciprocal interaction between cells and their microenvironment influence cellular adaptation to external mechanical cues through the remodeling of cytoskeletal structures and cell–matrix adhesions to ensure normal cell function. We proposed to investigate the relationship between the cytoskeletal tension development and cell adhesion to the matrix in the context of cellular contraction and migration. Our studies aimed to understand how cells sense, respond, and adapt to external mechanical forces in order to induce vascular remodeling in cardiovascular disease.

Integration of atomic force microscopy with total internal reflection fluorescence and spinning-disk confocal microscopy enabled acquisition of complementary structural and functional measurements on live vascular smooth muscle cells expressing key mutant proteins with important roles in defining contractile and migratory cellular properties.

Single ligand–receptor interaction measurements showed that RhoA and c-Src activation have different effects on cytoskeletal tension development, inducing two distinct force–stiffness functional regimes for $\alpha_5\beta_1$-integrin binding to fibronectin. In addition, c-Src was associated with regulation of myosin light chain phosphorylation, suggesting a c-Src-dependent modulation of RhoA pathway through activation of downstream effectors. These data were in good agreement with fluorescence measurements that

showed a modest effect of Src activation on stress fibers formation, in contrast with RhoA activation that had a significant effect. On the other hand, α-actin null cells exhibited increased FAK activation and cell stiffness. Our results suggest that the absence of α-actin may induce compensatory effects of up-regulation of other contractile proteins and activation of focal adhesion proteins in order to encourage cell migration and proliferation. In addition, our findings suggest that Nck regulates directional cell migration in part through modulation of cytoskeletal tension and cell-matrix adhesion strength, which has an important role in coordination of cytoskeletal mechanics through a mechanism that also involves the RhoA pathway.

Thus, our findings suggest that the contractile state of the cell is determined by cytoskeletal tension, which is controlled by a regulatory network involving RhoA and activation state of actomyosin apparatus. In turn, the cytoskeletal tension state modulates integrin $\alpha_5\beta_1$–fibronectin adhesion force. The results of this study suggest a central role for cytoskeletal tension in modulating cytoskeletal dynamics and cell adhesion to the matrix.

DEDICATION

Dedicated to my parents, Smt. Padmavathi and Shri. Sreenivasappa

ACKNOWLEDGMENTS

"Wherever I have knocked, a door has opened. Wherever I have wandered, a path has appeared". ~Alice Walker

I would like to express my deepest gratitude to my advisor, Dr. Andreea Trache, for the opportunity, patience and mentoring. Her infectious drive, encouragement, and faith in me have made me grow and push my limits to reach new heights. She has not only encouraged me to do good science but also inspired me give back to the community. I would like to extend my sincere gratitude to my committee members Dr. Wonmuk Hwang, Dr. Alvin Yeh, and Dr. Robert Burghardt for always encouraging and being excited about my work. I would also like to recognize and acknowledge my advisor's NSF CAREER grant for funding my research and me for the past 5 years and the Texas A&M University Dissertation Fellowship for supplementing my funding in my final year.

I convey my appreciation to our collaborators, Dr. Jerome Trzeciakowski, Dr. Warren Zimmer, Dr. Gonzalo Rivera, Dr. Emily Wilson, Dr. Dianna Milewicz, and Dr. Christopher Woodman for their amazing expertise, willingness to share, guidance, and encouragement. I would also like to recognize and thank Dr. Michael Davis, Dr. Michael Davidson, Dr. Benjamin Geiger, Dr. Kenneth Yamada, and Dr. Marilyn Resh for generously sharing reagents.

I am deeply grateful to Dr. Soon-Mi Lim for training me with all of the methods and also for her patience during this training. All of her graduate school survival tips were invaluable, as were the great laughs that lightened long days in the lab. I would also like to acknowledge Dr. Sankar Chaki from the Rivera Lab for his contribution with western blots and plasmid preparation. I am grateful to Dr. William Hyman for opportunity to publish my first paper during my Ph.D.

To all of my lab members - Anna Webb, Samuel Padgham, John Seawright, Matthew Tribble, Katelyn Wilson, Matthew Johnson and Stephen Johnson - thank you for giving me a lively lab environment to work in and helping with so much of the everyday lab stuff. Many thanks to Dr. Cindy Meininger, Katherine Kelly, and Jan Patterson for guidance with cell culture. I would also like to acknowledge Lin Bustamante from VIBS Histology Laboratory at Texas A&M University for preparing our histology slides.

Special thanks to the smiling and ever helpful Tina Mendoza, Stephanie Hilliard, Dr. Fidel Fernandez, and Maria Lyons for keeping me on track with all the academic paperwork, and for the great conversations.

I would like to take this opportunity to also thank all the faculty, staff, and students of both the Department of Biomedical Engineering and the Department of Medical Physiology. I would like to thank my doctor, Shikha Bharaktiya, for her guidance and support through my journey toward better health during my Ph.D. Many thanks to my

friends: Divya Natarajan, Rashmin Asher, Nandita Gaur, Dr. Katharine Prem, Vikram Mukku, Akilaesh Pandey, Dr. Champa Joshi, Pranalika Shinde, Jincy George, Khyathi Ruperalia and Padmaja Pancharatnam for being with me through this journey.

Finally, I am forever indebted to my loving family for being my inspiration, strength and calm during this challenging doctoral project. Thank you Padmavathi, Sreenivasappa and Shylendra for the unflinching support and love.

Thank you for a fantastic learning experience!

TABLE OF CONTENTS

Page

LIST OF FIGURES

Page

LIST OF TABLES

Page

NOMENCLATURE

AFM	Atomic Force Microscopy
CA	Constitutively Active
CCD	Charged-Coupled Device
DN	Dominant Negative
EC	Endothelial Cells
ECM	Extracellular Matrix
EGFP	Enhanced Green Fluorescent Protein
EYFP	Enhanced Yellow Fluorescent Protein
FA	Focal Adhesion
FAK	Focal Adhesion Kinase
FN	Fibronectin
FRET	Förster Resonance Energy Transfer
GAPDH	Glyceraldehyde 3-Phosphate Dehydrogenase
GDP	Guanosine Diphosphate
GEF	Guanine Nucleotide Exchange Factor
GFP	Green Fluorescent Protein
GTP	Guanosine Triphosphate
H&E	Hematoxylin and Eosin
LPA	Lysophosphatidic Acid
LN	Laminin

MLC	Myosin Light Chain
mRFP	Monomeric Red Fluorescent Protein
MRLC	Myosin Regulatory Light Chain
NA	Numerical Aperture
pFAK	Phosphorylated Focal Adhesion Kinase
pMLC	Phosphorylated Myosin Light Chain
pTyr	Phosphotyrosine
ROCK	Rho Kinase
TIRF	Total Internal Reflection Fluorescence Microscopy
TMLC	Total Myosin Light Chain
TRI	Masson's Trichrome
VSMC	Vascular Smooth Muscle Cell
VVG	Verhoeff-Van Gieson
wt	Wild type

1 INTRODUCTION

The cell is the fundamental unit of life. In a multicellular organism, cells are organized into tissues and organs to perform specific functions. Cells are embedded in a three-dimensional extracellular matrix (ECM) composed of extracellular proteins and glycoproteins. Mechanical forces, either in the form of external forces that are applied to tissues, or endogenous forces that are ever-present, modulate reciprocal interaction between the cells and the ECM to facilitate tissue organization and integrity (Ingber, 1998; Jaalouk and Lammerding, 2009; Tschumperlin, 2011). Furthermore, these mechanical forces regulate the expression of specific genes and proteins, giving the cells in the tissues their inherent characteristics (Chen, 2004; Chen, 2008; Ingber, 1998). Changes in these mechanical forces disrupt the physiological function and contribute to various pathologies (Chen, 2008, Hahn and Schwartz, 2009; Jaalouk and Lammerding, 2009). The process by which cells sense mechanical cues from the environment and convert them to biochemical signaling processes is termed mechanotransduction.

Alterations in composition and structure of the vessel wall lead to progressive changes in mechanical forces in that wall, resulting in cardiovascular pathology. We were interested in understanding the effect of microenvironmental stresses on cell behavior in the context of cardiovascular disease. Our study will fill a gap in the current knowledge regarding VSMC mechanotransduction by elucidating the mechanisms through which

cells sense and adapt to the mechanical cues from the environment in cardiovascular disease at the subcellular level.

Section 2 highlights the significance of our study and gives a brief background on vascular wall mechanics, including the role of vascular smooth muscle cells. It also looks at the importance of RhoA pathway modulation in cardiovascular disease.

Section 3 describes our experimental approach and the integrated microscope set-up used to perform experiments. This section includes a detailed presentation of each microscopy technique and highlights the innovation of the work.

Section 4 presents the experimental results of our study. First, we discuss the role of RhoA-Src crosstalk on cytoskeletal tension and cell-matrix adhesion. Second, we discuss the effect of loss of α-actin on cytoskeletal tension, cell migration, and proliferation. Lastly, we discuss the role of Nck modulation on cytoskeletal tension and adhesion strength in the context of directional cell migration.

Section 5 summarizes the study by highlighting key findings; we also discuss future directions of the study.

Section 6 describes in detail the experimental methods, including cell culture, sample preparation, and molecular methods used for this study.

2 BACKGROUNDS AND SIGNIFICANCE

Cardiovascular disease is the leading cause of death in the US. It accounts for 40% of all the deaths in the US, more than all forms of cancer combined (Go et al., 2014). One in three adults have one or more types of cardiovascular disease. Impaired vasculature composition and function are linked with most cardiovascular diseases. For example, hypertension, which is one of the main risk factors for cardiovascular disease, is characterized by increased vascular resistance due to smooth muscle cell hyperactivity and excess deposition of extracellular matrix (ECM) in the vessel wall (Lee et al., 1998). In addition, vessel wall remodeling alters vascular tone, which leads to atherosclerosis due to narrowing of the blood vessels, making them more likely to block from blood clots. In 2013, the American Heart Association estimated 78 million U.S. adults were hypertensive (Go et al., 2014), which represents 32% of the US population.

Genetic mutations also trigger vasculature disruption and lead to cardiovascular disease. Mutations in ACTA2, a smooth muscle cell specific α-actin isoform, are known to induce hyperplasia of VSMC in the neointimal or medial layers of the arteries (Guo et al., 2007). This mutation can induce occlusive vascular diseases like thoracic aortic aneurysms, acute aortic dissections, early onset coronary artery disease, stroke, and primary pulmonary hypertension (Guo et al., 2007; Guo et al., 2009; Milewicz et al., 2010).

2.1 Vessel Wall Mechanics

Blood vessels are continually subjected to cyclic stretch and shear stress generated by systemic hemodynamics (Pries and Secomb, 2002). Precise control of hemodynamics under different conditions ranging from strenuous exercise to complete rest is ensured through multiple mechanisms that carefully regulate blood pressure (Beevers et al., 2001). These are accompanied by changes in luminal diameter due to adaptation of vascular tone and vascular structure (Pistea et al., 2005).The vascular myogenic response represents the mechanism by which resistance vessels constrict in response to increased intravascular pressure and dilate in response to a reduction in pressure (Orr et al., 2006). Normal hydrostatic pressure in blood vessels promotes maturation of vascular smooth muscle cells (VSMC), whereas chronic increase in pressure causes blood vessel walls to thicken (Beevers, 2001; Weber et al., 1989; Westerhof and O'Rourke, 1995). Similarly, blood flow-induced shear stress prevents activation of coagulation cascades within the blood vessel and helps maintain endothelium in an anti-inflammatory and anti-atherogenic state (Cines et al., 1998; Gimbrone et al., 1999). Even with extensive studies demonstrating that mechanical cues govern signaling and function of cells, the mechanism of how cells sense the mechanical stimuli and convert them to biochemical signaling processes (i.e., mechanotransduction) is not completely understood.

Arterioles are small blood vessels that form the major resistance component of the vasculature and are the most sensitive to pressure. The arteriole wall consists of three layers: the tunica intima with one layer of endothelial cells (EC) supported by a basal

lamina, the tunica media with circumferentially orientated VSMC, and the tunica adventitia with connective tissue containing fibroblasts (Halka et al., 2008). *In vivo*, EC are directly exposed to shear stress resulting from blood flow, while VSMC embedded in the ECM in the vessel wall are mainly subjected to the cyclic stretch of pulsatile blood pressure that deforms the ECM and induces axial and circumferential wall stresses (Figure. 1). In response, VSMC adapt to the mechanical factors by remodeling their cellular structure and altering signaling transduction pathways (Halka et al., 2008; Pries and Secomb, 2002), contributing to the regulation of the vascular myogenic responses.

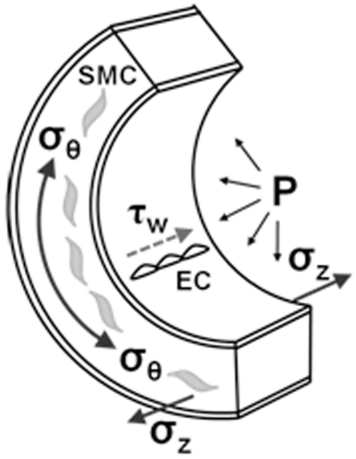

Figure 1: Vascular wall cross-section.
Distribution of mechanical stresses in the vascular wall in vivo: τ_z – axial wall stress; τ_y – circumferential wall stress; τ_w – shear stress. (Reproduced by permission of The Royal Society of Chemistry from Lim et al., 2012, doi: 10.1039/c2ib20008b)

Under normotensive conditions the magnitude of wall stress measures ~ 40-60 kPa, but easily exceeds 100 kPa during hypertension (Humphrey et al., 2009; Shadwick, 1999).

This increase in pressure impairs the ability of the blood vessel to locally control blood flow, and it triggers a compensatory hypertrophic or hyperplastic vessel wall remodeling response to regain this ability (Engler et al., 2009; Farr et al., 2009; Orr et al., 2006; Tyler, 2012; Van Vliet et al., 2003)

Our study focuses on VSMC, a fundamental contributor to vessel wall homeostasis, which plays an important role in compensatory adaptations of the vessel wall to altered loads. Thus, VSMC provide an excellent model system to study the mechanotransduction process.

2.2 Main Contributors to Vessel Wall Remodeling

2.2.1 Matrix of the vessel wall

The ECM constitutes an intricate network of macromolecules surrounding the cell (Wagenseil and Mecham, 2009). The vessel wall is composed of structural matrix proteins, like collagens (Coll I and Coll IV) and elastin, and functional proteins, like fibronectin (FN) and laminin (LN) (Davis et al., 2001; Glukhova and Koteliansky, 1995; Lim et al., 2010). Figure 2 shows the histology of thoracic aorta cross sections stained with hematoxylin and eosin (H&E) for general morphology, Verhoeff van Gieson (VVG) for elastin, and Masson's trichrome (TRI) for collagen. The matrix composition plays a major role in defining the viscoelastic properties of the vessel wall. Elastin protein forms extracellular extensible fibers (elastic fibers) that give tissues the ability to recoil after transient stretch. Coll I are rod-like proteins that assemble to form fibers.

These fibers then form the insoluble three-dimensional framework of any tissue, thus determining its mechanical properties. In vasculature, collagen contributes to the tensile strength of the vessel wall (Sharf et al., 1998; Stehbens and Martin, 1993). The ratio of inelastic collagen and elastin together determine the vessel wall compliance (VanBavel, et al., 2003).

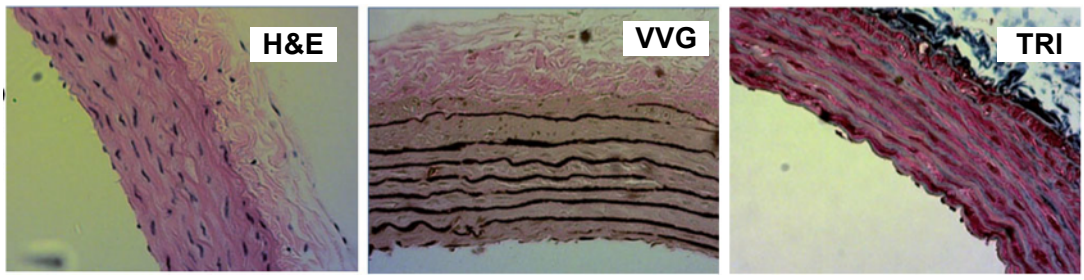

Figure 2: Histology of thoracic aorta cross-sections.
Tissues were stained with H&E to show the tissue morphology (hematoxylin for cytoplasm, and eosin for nuclei), VVG for elastin, and TRI stain for collagen.

LN and Coll IV are essential structural components forming the basal lamina, which has the role of stabilizing the vessel wall. FN helps the cell attach to the matrix through integrins. Each FN has a major site for integrin binding called the Type III FN repeat – it contains the Arg-Gly-Asp (RGD) sequence and its synergy site (Friedland et al., 2009). FN plays an important role in regulating VSMC adhesion to the matrix (Chiang, et al., 2009; Ruoslahti, 1996).

2.2.2 Vascular smooth muscle cells

2.2.2.1 Cell-matrix adhesions

Integrins are transmembrane heterodimeric proteins found in cell membrane that physically link the ECM to the cell. The integrin is composed of two covalently bound alpha and beta subunits. 18 types of α-subunits and 8 types of β-subunits are known to group together to form 24 distinct integrins (Hynes, 2002; Srichai and Zent, 2010). Each integrin is structured to have an extracellular domain to facilitate binding to the extracellular environment, a transmembrane domain, and a small cytoplasmic tail region. The cytoplasmic tail domain binds to actin filament via a complex of intracellular attachment proteins called focal adhesion (FA) proteins (Petit and Thiery, 2000; Romer et al., 2006; Zaidel-Bar R et al., 2007; Zaidel-Bar R and Geiger, 2010). VSMC predominantly express integrins $\alpha_5\beta_1$, $\alpha_1\beta_1$, $\alpha_2\beta_1$, $\alpha_4\beta_1$, and $\alpha_v\beta_3$ corresponding to fibronectin, collagens, and laminin found in the vessel walls (Davis et al., 2001; Glukhova and Koteliansky, 1995; Lim et al., 2010). The extracellular domain of the integrin binds to specific amino acid sequences presented by specific ECM proteins. Integrins $\alpha_5\beta_1$ and $\alpha_v\beta_3$ are involved in the regulation of contractile function (Martinez-Lemus et al., 2005; Martinez-Lemus et al., 2009; Martinez-Lemus et al., 2003). $\alpha_5\beta_1$ binding to the RGD recognition sequence in ECM proteins induces vascular contraction (Wu et al., 1998; Wu et al., 2001), while $\alpha_v\beta_3$ binding to the same ligand causes arteriolar relaxation (D'Angelo et al., 1997; Mogford et al., 1997). However, both

integrins are needed for blood vessel vasoconstriction in response to increased pressure (Martinez-Lemus et al., 2004).

Integrin affinity to its ligand is determined by its conformation state. In the resting state, integrins have low affinity to their ligands (Takagi et al., 2002). However, the integrins can be activated either by inside-out signaling or outside-in signaling. In inside-out signaling, the integrin switches to a higher affinity binding state due to cytoplasmic events such as talin binding to the β integrin tail (del Rio et al., 2009; Tadokoro et al., 2003). Conversely, in the outside-in activation, extracellular factors such as the ligand binding to the extracellular domain of integrin can result in integrin activation. Thus, the unique structure of integrin facilitates bidirectional signaling across the cell membrane, such that the integrin functions as a mechanotransducer.

The overall strength of cell-matrix adhesion is governed by integrin affinity and integrin avidity. Avidity is defined as the lateral mobility and clustering of integrins in the plane of the membrane (Schwartz and Shattil, 2000). Affinity modulation is regulated by the intracellular signaling events that remodel cytoskeletal linkages, which influence adhesion strength to the extracellular ligand. Affinity and avidity modulation play complementary roles in regulating the activation of integrins.

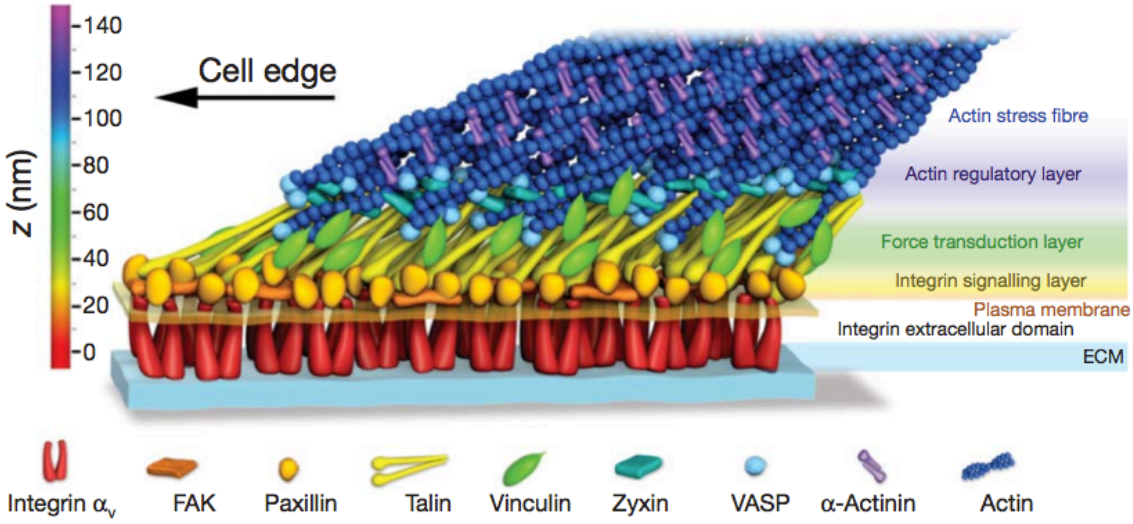

Figure 3: Nanoscale architecture of focal adhesions.
Schematic model of focal adhesion molecular architecture, depicting experimentally determined protein positions. (Reprinted from Kanchanawong et al., 2010 with permission from Nature Publishing Group).

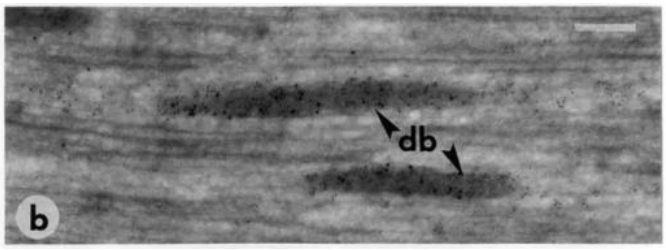

Figure 4: Longitudinal cryosection of immuno-electronmicroscopy of smooth muscle showing specific localization of α-actin β-cytoplasmic actin (5nm gold particles) in dense bodies.
β-cytoplasmic actin was also present in the cytoskeletal channels that link them. Scale bar is 0.2 mm. (Reprinted from Small and North, 1995 with permission from Elsevier)

A focal adhesion complex includes structural proteins (like talin, α-actinin, and vinculin), adaptor proteins (like paxillin and zyxin), and signaling proteins (like focal

adhesion kinase (FAK)), to name only a few out of the 905 identified FA associated proteins—459 of which represent the myosin-II responsive FA proteome (Figure 3) (Kanchanawong et al., 2010). These dynamic structures assemble, disperse, and turnover in response to mechanical force, representing critical sites for cell attachment to matrix (Chen et al., 2004; Dubash et al., 2009; Parsons et al., 2010; Petit and Thiery, 2000; Romer et al., 2006; Sastry and Burridge, 2000).

The function of FA have been extensively studied in fibroblasts, however little is known about FA physiology specific to VSMC (OpazoSaez et al., 2004; Worth et al., 2001). The VSMC FA structure seen on a 2D-cell culture is analogous to the "dense plaques" observed in smooth muscle *in vivo* (Figure 4), identified as a junction between the ECM on the outside of the cell and the contractile cytoskeleton on the inside (Turner et al., 1991). These dense plaque regions have been shown to be rich in contractile and FA proteins (Gunst and Zhang, 2008; Turner et al., 1991). For this reason, studying VSMC in culture is relevant for understanding ECM effects on FA and actin stress fiber formation (Morgan et al., 2007) *in vivo*. Figure 5 shows the differential localization of FA proteins in VSMC.

Thus, integrin-mediated cell-matrix adhesions trigger cytoskeletal changes that drive adaptive cellular responses to enable a functional vasculature (Zhang and Gunst, 2006).

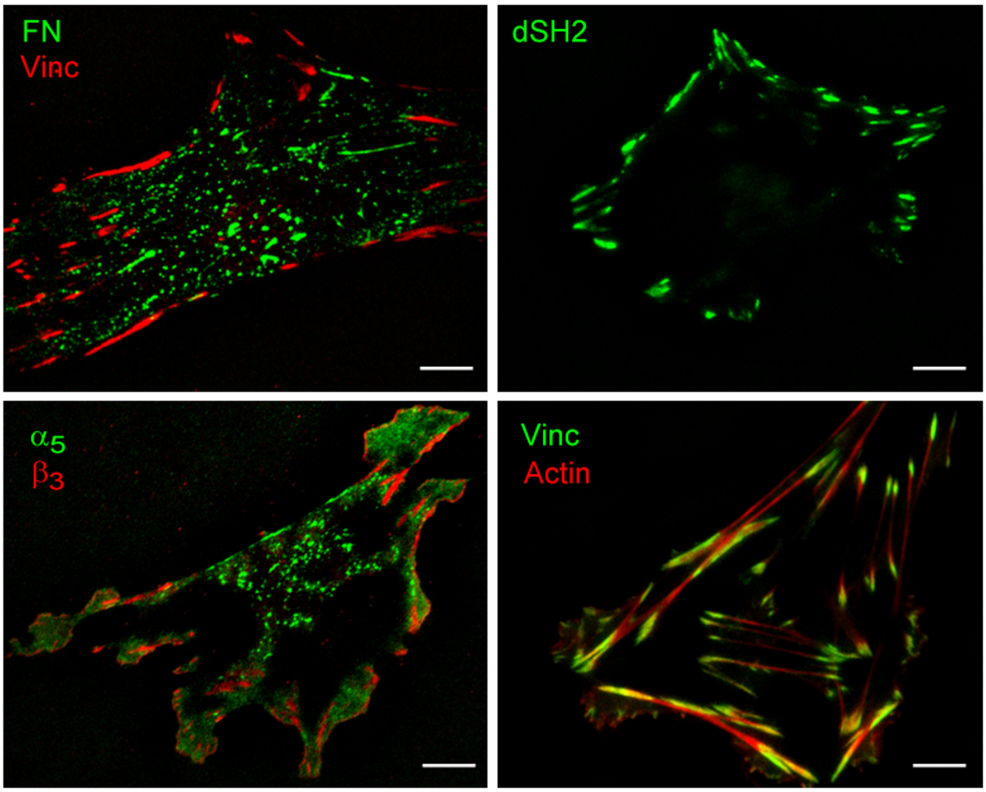

Figure 5: Differential localization of protein at the basal surface of VSMC.
Total internal reflection fluorescence (TIRF) images of VSMC showing (a) Endogenous fibronectin (FN) localized mainly inside the cell while vinculin (Vinc) is localized at the cell edges (b) Tyrosine phosphorylation (dSH2) observed mainly at the edges of the cell. (c) Integrin β_3 is localized mainly at the edges while α_5 localization is all over the basal cell surface similar to that of endogenous fibronectin. (d) Actin and vinculin localization is all over the basal surface of the cell. Scale bar represents 10 μm

2.2.2.2 Cytoskeleton

The integrity of the structure, shape, and mechanical properties of the cell is maintained by the dynamic cytoskeletal filaments composed of actin filaments, microtubules, and intermediate filaments. Within the cell, these dynamic filamentous protein structures are

in isometric tension, such that some of the structures are in tension while others are in compression (Ingber, 2006). The cytoskeleton constantly remodels to maintain the force balance necessary for giving strength and structure to the cell.

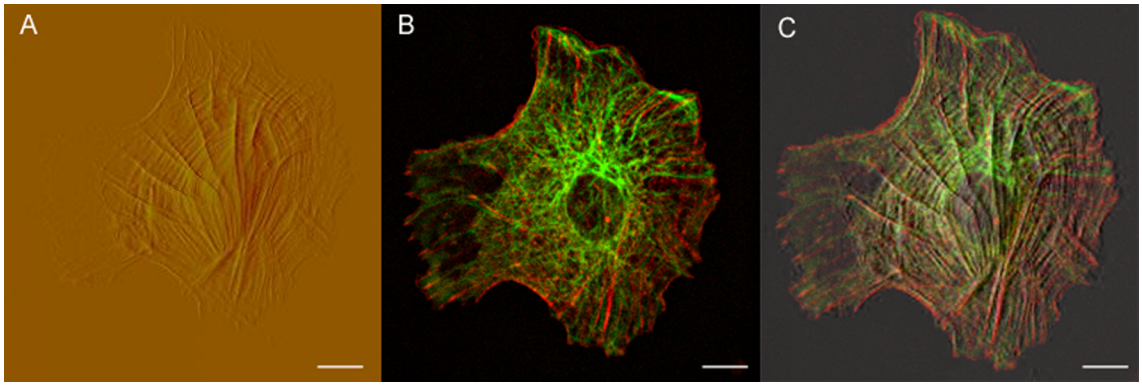

Figure 6: Actin and microtubules in VSMC.
(A) Atomic Force Microscope (AFM) showing the cytoskeleton in the apical surface of the cell, (B) confocal image of a live VSMC co-transfected with GFP-tubulin and mRFP-actin, and (C) overlay of the confocal and AFM image. Scale bar represents 10 μm.

Actin is the key modulator of contractility and cytoskeletal tension in VSMC. An actin filament is composed of 2α–helical strands of actin monomers, and is crucial in determining cell shape and motility. Actin filaments are organized differently across the cytoplasm (Figure 6). Actin filaments of the same polarity are closely spaced to form the linear bundles found in the filopodia, while loosely spaced filaments of opposite polarity form the contractile bundle, also known as stress fibers. Actin filaments can also form

gel-like networks, with filaments arranged loosely via orthogonal interconnections, which are localized in lamellipodia (Borisy and Svitkina, 2000).

Microtubules are hollow cylinder-like structures made of tubulin dimers with one end connected to the centrosome and the other pointing toward the cell edges (Figure 6). They serve as tracks for molecular motors (dynein and kinesin) to deliver membrane vesicles and proteins. These highly dynamic structures also play a fundamental role in cell division, cell shape changes, and motility (Etienne-Manneville, 2010; Lansbergen and Akhmanova, 2006). Intermediate filaments are rope-like structures that form an elaborate network in the cytoplasm. They give mechanical strength to the cell and maintain its structural integrity (Eriksson et al., 2009; Herrmann et al., 2009)

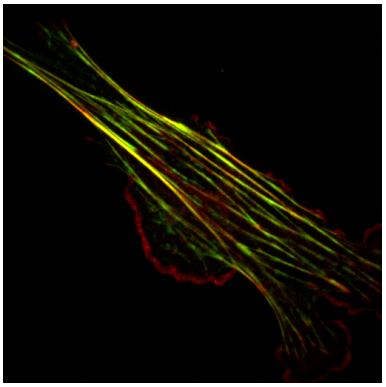

Figure 7: Actin and myosin regulatory light chain (MRLC) in VSMC.
Confocal image of live VSMC expressing MRLC-GFP and actin –mRFP shows a relative overlap of myosin with actin.

The actin filaments anchor the cell to the ECM and neighboring cells through cell-matrix adhesion and cell-cell adhesion, respectively. The mechanical stimuli externally applied

to the cell are recognized by the mechanosensitive adhesion molecules and the force is subsequently transduced across the cell through the actomyosin cytoskeletal network (Figure 7). Consequently, the contractile apparatus balances the external mechanical force by intracellular counter-forces generated by myosin.

2.3 Role of RhoA in Mechanotransduction

RhoA is a small G protein that belongs to the family of Rho GTPase. RhoA cycles between GTP-bound (guanosine triphosphate) active and GDP-bound (guanosine diphosphate) inactive form. In physiological conditions, RhoA activity is necessary for homeostatic function of VSMC. RhoA pathway is activated due to stimuli such as growth factors, or hormones (Huveneers and Danen, 2009; Kjoller and Hall, 1999).

Rho-kinase (ROCK) is identified as a key effector downstream of RhoA. ROCK activation promotes calcium-independent contraction (Bi et al., 2005; Van Eyk et al., 1998), actin polymerization (Maekawa et al., 1999; Watanabe et al., 1999), and myosin phosphorylation (Amano et al., 1996; Woodsome et al., 2006). Increased stress fiber formation and myosin contractility trigger maturation of focal adhesions (Burridge and Wennerberg, 2004; Ridley and Hall, 1992). Thus, the RhoA/ROCK pathway is important for regulation of VSMC adhesion, differentiation, and migration by controlling cytoskeletal assembly and cellular contractility (Zhou and Liao, 2009). Consequently, sustained over-activation of RhoA-dependent pathways leads to the vascular wall remodeling characteristic of cardiovascular pathologies like hypertension

and atherosclerosis (Loirand and Pacaud, 2004; Nunes et al., 2010; Rolfe et al., 2005).

The role of ROCK as a pharmacological agent has been extensively studied (Bolz, et al. 2003; Gokina et al., 2005; Narumiya et al., 2000; Wirth, 2010). In both animal models and human patients with hypertension, treatment with Y-27632, a specific Rho-kinase inhibitor, is shown to have a protective effect as it induces a decrease in VSMC proliferation and contraction (Wirth, 2010; Zhou and Liao, 2009).

In conclusion, RhoA pathway is an important regulator of load-bearing components of the cell (i.e., cytoskeleton and focal adhesion). We studied the role of RhoA in modulating the cytoskeletal tension, adhesion force, and consequent cellular remodeling. Correspondingly, we further studied the effects of Src, Nck (non-catalytic region of tyrosine kinase), and alpha-smooth muscle actin on RhoA pathway modulation subsequently induced cytoskeletal tension.

3 EXPERIMENTAL SETUP

Our study used an across-scales experimental approach from single molecule to live VSMC in culture, with the aim of understanding show cells sense, respond, and adapt to external mechanical forces in order to induce vascular remodeling in cardiovascular disease.

The advantages of our experimental approach are:

- Single-cell experiments can be used to dissect the mechanical pathways that alter microscopic behavior in a way that is not possible to study at the tissue level.
- Studying the mechanical effects at the cellular level will help understand and predict changes at the macroscopic tissue level.
- Unlike using fixed cells where the information is obtained at a specific time point, live-cell studies facilitate continued observation of cell behavior in real-time.
- This unconventional integrated experimental approach employs the power of an integrated atomic force microscope (AFM) combined with total internal reflection fluorescence (TIRF) and fast spinning-disk confocal microscopy. Thus, AFM is able to mechanically stimulate live cells while ***simultaneous*** measurements of cellular remodeling to the applied force are recorded by optical imaging.

Although the mechanotransduction process has been extensively studied, the basic molecular mechanism that drives this process remains elusive. To understand how cells respond to mechanical forces we investigated focal adhesion and cytoskeletal remodeling in VSMC in culture.

3.1 Microscopy

3.1.1 Novelty of integrated microscopy system

The use of innovative and unconventional imaging techniques has been critical for deeper understanding of the biological process since the introduction of the microscope to life science by Robert Hooke in 1665 (Hooke, 1665). Development in the fields of optics, electronics, lasers, fluorescent probes, and detection devices has further revolutionized experimental capabilities in terms of accuracy, speed, selectivity, and resolution (Bertocchi et al., 2013; Han et al., 2013; Nienhaus and Nienhaus, 2014).

Cells continually assemble and turnover their dynamic structures (i.e., cytoskeleton and focal adhesions) to maintain the intra-cellular force balance in response to microenvironmental mechanical forces. To dissect the underlying mechanism of mechanotransduction processes in live cells we need a microscopy technique that is able to capture this structural remodeling of the cell along with the functional adaptation of the cell.

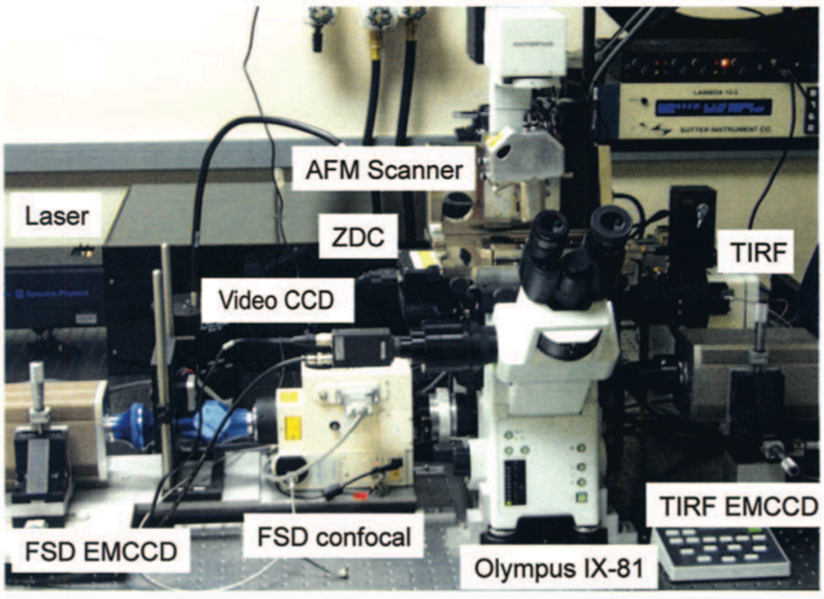

Figure 8: Layout of integrated microscope system.
(Reproduced with permission from Trache and Lim, 2009)

To make these experiments possible, we used an integrated microscopy system (Figure 8) that combines TIRF, spinning disk confocal, and AFM (Trache and Lim, 2009). Each of these techniques was combined to complement each other and maximize the information obtained from the sample. TIRF is confined to the basal surface of the cell, while the spinning-disk confocal is able to examine cytoplasmic volume with rapid optical sectioning. AFM not only gives detailed topographical information but is also able to sense or mechanically stimulate the cell with forces in the pico- to nano-Newton scale (Trache and Lim, 2009). This integrated system enabled us to capture and correlate structural and functional cellular characteristics in order to study the eventual crosstalk between biochemical pathways that are spatio-temporally regulated in living cells.

3.1.2 Atomic force microscopy

AFM is a type of scanning probe microscopy that generates images by "feeling" rather than "looking" at the sample. Binnig, Quate and Gerber combined the principles of scanning tunneling microscopy and stylus profilometer to develop AFM (Binnig et al., 1986). AFM was further adapted to biological applications (Lal and John, 1994; Radmacher et al., 1992) due to its remarkable capacity to interact with biological samples in their physiological environment with nanometer resolution. This novel technique enables topographical imaging of live cells, as well as single ligand-receptor force measurements between proteins coated on the AFM probes and receptors endogenously expressed on the cell surface. In addition, AFM can be used as a nano-manipulation tool to mechanically stimulate the cells (Lim et al., 2012; Sun et al., 2012). Thus, AFM provides structural and functional information with high resolution under physiological conditions.

3.1.2.1 Principle of operation

The operating principle of AFM is very similar to that of a record player or a stylus profilometer (Binnig et al., 1986; Morris et al., 1999). Unlike light microscopy that collects and focuses light, AFM uses a sharp cantilever tip to interact with the sample and sense the local forces in order to map the topography at a resolution below the diffraction limit. Consequently, the resolution of AFM is limited by the tip radius and spring constant of the cantilever (Braga and Ricci, 2004).

Figure 9 shows the schematic diagram of an AFM system. AFM has a sharp tip mounted on a soft cantilever that is raster scanned across the surface of the sample using a piezo scanner and a detection mechanism that senses the forces between the sample and the tip. The detection mechanism consists of an optical lever system that utilizes a laser beam reflected off the backside of the cantilever tip onto a detector to record the deflection of the tip as the tip scans across the sample. In addition, the feedback mechanism of the piezo scanner records the changes in the forces between the sample and tip (Trache and Meininger; 2008a).

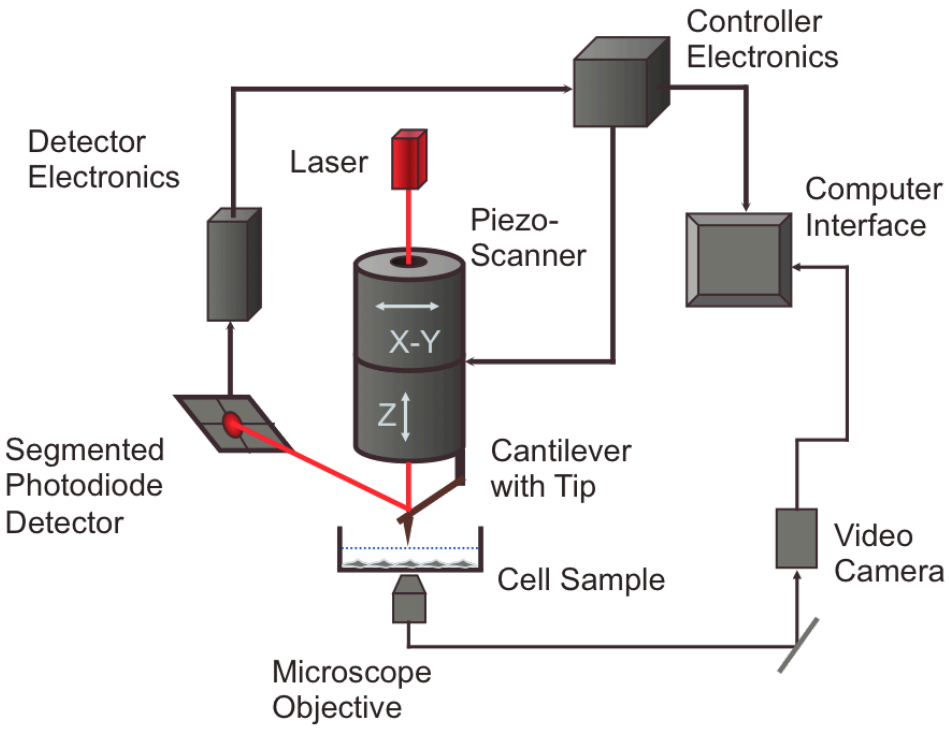

Figure 9: Schematic representation of the AFM system.
(Adapted from Trache and Meininger, 2008a).

Probe geometry and its material properties play an important role in defining the sensitivity of the system. For example, the radius of the tip limits the resolution of imaging while the softness of the spring constant of the cantilever limits the magnitude of stiffness and forces detected. Most common probes are microfabricated using silicon nitride or silicon. The AFM tip is chosen based on the application. For cell imaging and force measurements a pyramidal shaped tip with a tip radius of 20-60 nm mounted at the end of a 'V' shaped cantilever with a spring constant of about 12 pN/nm is used. However, a glass bead tip of 2-5μm radius attached to a tip-less 'V' shaped cantilever with the same parameters is used for mechanical manipulation.

AFM can be operated in different modes such as contact or tapping mode (Morris et al., 1999; Putman et al., 1994) to interact with the sample. For all our experiments we use contact mode where the tip remains in contact with the sample at all times.

3.1.2.2 Applications

AFM is a versatile, precision tool that can be used for different applications: (1) topographical imaging, (2) adhesion and molecular recognition, and (3) tensile force application.

3.1.2.2.1 Imaging in contact mode

Contact mode is a common imaging mode also known as the constant force mode. The tip is brought into contact with the sample and maintained at a 'pre-set' constant deflection (force) while raster scanning across the sample in x-y axis. The feedback loop

constantly adjusts the z scanner with respect to the topographical height to maintain the 'pre-set' force of the cantilever. The z-scanner captures the true height of the sample at each x-y coordinate, while the cantilever deflection records the finer topographical details (Figure 10) (Trache and Meininger, 2008a).

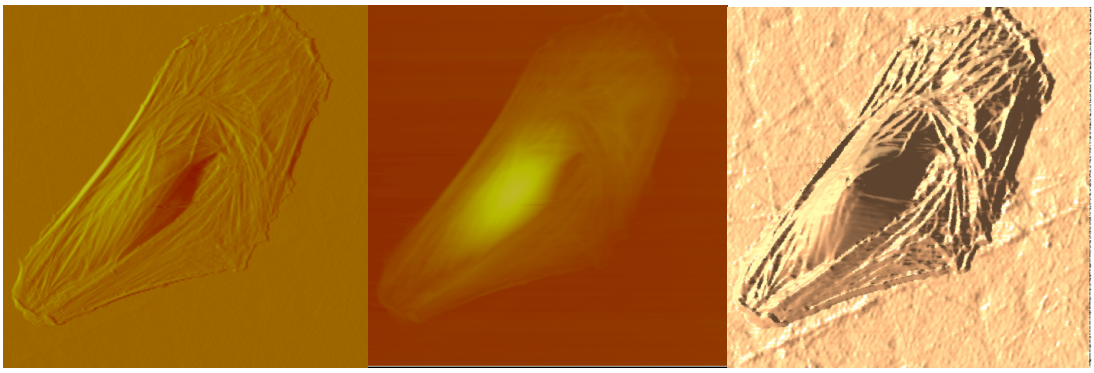

Figure 10: AFM image of VSMC.
(A) Deflection image (from optical lever) of the cell showing detailed topography of the apical surface of the cell. (B) True height image (from piezoscanner) of the same cell. (C) Reconstructed 3D image from height image.

3.1.2.2.2 Adhesion force spectroscopy

AFM operated in force mode can be used to study local chemical and mechanical properties like adhesion and elasticity. In force mode, the piezo element is set to drive from a predefined distance in the z direction at a constant frequency. The tip is brought in contact with the sample, eventually indents the surface, and is then retracted to the

original position. Concurrently, z-axis movement of the piezo and the deflection of the cantilever are recorded in a force curve.

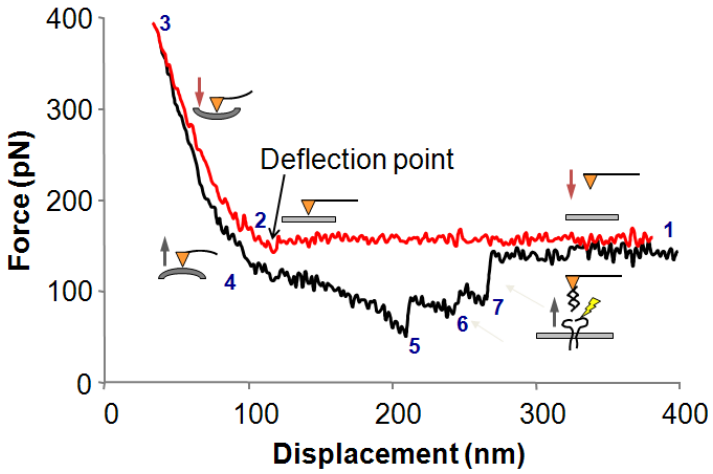

Figure 11: Experimental AFM force curve.
The above picture represents one force curve pair with the approach curve (in red) and retraction curve (in black). The x axis represents the piezoelectric element displacement and the y axis represents the force calculated from the photodetector signal. The AFM probe labeled with fibronectin is driven at a constant frequency to touch and retract from the cell. Right to left, (1-2) as the AFM tip approaches the cell from a predefined distance, the detector records a constant deflection signal. At (2) is the deflection point where the AFM tip makes contact with the cell. (2-3) the tip is further indented into the cell, the tip bends, and the deflection signal increases. (3-4) the tip is retracted from the surface and the deflection signal decreases. (5-7) Adhesions formed between the fibronectin on the tip and integrins rupture and the cantilever returns to the original position (1) (Adapted from Trache and Meininger, 2008a).

A typical force curve is shown in Figure 11, where the tip approaches the cell (approach curve) from a pre-set distance in z-axis (1 to 2), contact is established (2) with the cell, and subsequently the cell surface is indented (2 to 3). However, further probe extension

into the surface is met with resistance from the cell with an opposing force of increasing magnitude. In response, the cantilever undergoes an upward deflection. The tip is then withdrawn (retraction curve) from the sample (3-4); if there is an adhesion between the tip and the sample, the cantilever bends downwards, resulting in a deflection signal lower than the original value (5). As the tip further retracts, all the adhesions are broken and the cantilever returns to the original position (1) (Trache and Meininger, 2008a).

Sneddon extended Hertz's analytical solution (Hertz, 1881) to elastic deformation that takes place between two spheres in contact under load to a cone indenting a flat surface (Sneddon, 1965). For AFM force spectroscopy, the probe was considered a cone and the curvature of the cell membrane at the point of contact is considered as a flat surface given the small area of the probe. To quantitatively calculate the elasticity of a sample with the AFM, the Sneddon-Hertz model is fitted to the portion of the approach curve between the initial point of cell contact and the point of maximal probe displacement. Assuming the cell is a homogeneous, flat, and elastic sample, the Sneddon-Hertz model (Sneddon, 1965) was applied to derive the apparent modulus of elasticity of the cell at the point of indentation (You and Yu, 1999). The loading force F is given by

$$F = \frac{2}{\pi}\frac{E}{1-\nu^2}\frac{\delta^2}{\tan\alpha} \text{ with } r_{cone} = \frac{2}{\pi}\frac{\delta}{\tan\alpha} \quad (1)$$

where, δ is the indentation into the cell body caused by the tip, E is Young's modulus of cell at the point of contact, α is the half angle of the indenting cone, and ν is the Poisson ratio of the cell, which is assumed to be 0.5. (Trache et al., 2005)

The z-displacement of the piezo and the cantilever deflection *d* were expressed relative to the point at which the probe tip contacted the cell surface (z_0, d_0). Therefore Eq 1 can be written as,

$$F = kd_m = \frac{2}{\pi}\frac{E}{1-\nu^2}\frac{(z_m - d_m)^2}{\tan\alpha} \quad (2)$$

where relative probe displacement is $z_m = z - z_0$ and relative probe deflection is $d_m = d - d_0$. Thus, the adhesion force (*F*) is calculated as the product between the deflection height associated with the unbinding event and the spring constant (*k*) of the cantilever. Rearranging Eq 2

$$d_m = \frac{2}{\pi}\frac{E}{k(1-\nu^2)\tan\alpha}(z_m - d_m)^2 \quad (3)$$

Knowing *k*, *v*, and α, elastic modulus can be determined by fitting the relationship between relative probe displacement and indentation (Trache et al., 2005)

3.1.2.2.3 Tensile stress application

The AFM was operated in contact imaging mode for tensile stress stimulation of cells. A glass bead probe, functionalized with matrix protein, was brought in contact with the apical cell surface and kept in contact for 20 mins. This is called the steady-state condition, and allows the matrix coated on the probe to initiate formation of a FA. The displacement vs. time dependence of the steady state condition is flat (Figure 12), because there is no tensile stress application to the cell. To further induce integrin

clustering, and recruitment of actin and other FA proteins, low-magnitude forces (< 0.4 nN) were applied in discrete steps during the priming period (Lim et al., 2012).

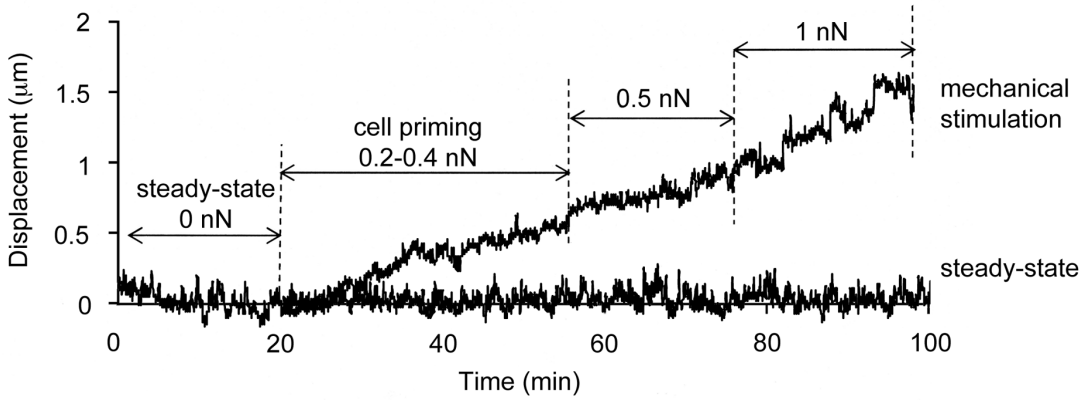

Figure 12: Representative experimental traces for the steady-state condition (lower trace) and a mechanical stimulation experiment (upper trace).
In the steady-state condition, the FN functionalized probe rests in contact with the apical cell surface without application of external forces. Thus, the displacement vs. time dependence is flat. The upper trace represents a single mechanical stimulation experiment that was divided into four segments based on the force regimes applied to the cell: steady-state (no force), cell priming (low force), and discrete step-force application at 0.5 and 1 nN (see text for details). (Reproduced by permission of The Royal Society of Chemistry from Lim et al., 2012, doi: 10.1039/c2ib20008b).

After the priming period, the live cell was mechanically stimulated through an active matrix-integrin-actin linkage by directly manipulating the cortical actin cytoskeleton, followed by downstream activation of the intracellular signaling pathways that eventually induces cellular remodeling and establishes a new homeostatic state. Each discrete force application to the cell was induced by an upward movement of the AFM probe (Figure 12), which corresponded to a specific voltage applied to the piezo. Mechanical stimulation of the cell at low (~0.5 nN) and high (~1 nN) magnitude forces

applied every 3–5 min for 20–25 min each was performed. Each discrete mechanical stimulation event was characterized by a step-displacement followed by the cell response under conditions of constant force application. Eigenvalue decomposition analysis was used to further process the series data for probe displacement versus time (Lim et. al., 2012). For the purpose of this work, we will present only the overall cell response over time (i.e., displacement over time), which was calculated by averaging the baselines for each treatment, and then fitting each average baseline with a quadratic function.

3.1.3 Total internal reflection fluorescence microscopy

TIRF is an optical microscopy technique that facilitates imaging below the diffraction limit of light in z-axis. It uses the principle of total internal reflection to excite and visualize fluorescent molecules in the near-membrane region of live cells in contact with a glass coverslip. This method was first introduced in 1965 by Hirschfeld (Hirschfeld, 1965), and it was further refined and adapted to life sciences by Axelrod in 1983 (Axelrod et al., 1983; Axelrod et al., 1984).

3.1.3.1 Principle of operation

TIRF is based on the phenomenon of total internal reflection that occurs when light propagates from a region of higher refractive index (n_1) to a region of lower refractive index (n_2). At an angle of incidence greater than the critical angle (θ_C) all the incident light gets reflected back into the higher refractive index region (n_1) (Figure 13).

At the interface of the two media, a short-range electromagnetic disturbance called evanescent wave propagates into the low refractive medium (n_2). For TIRF microscopy, this evanescent wave acts as a source of excitation for fluorescent probes (Axelrod, 2008).

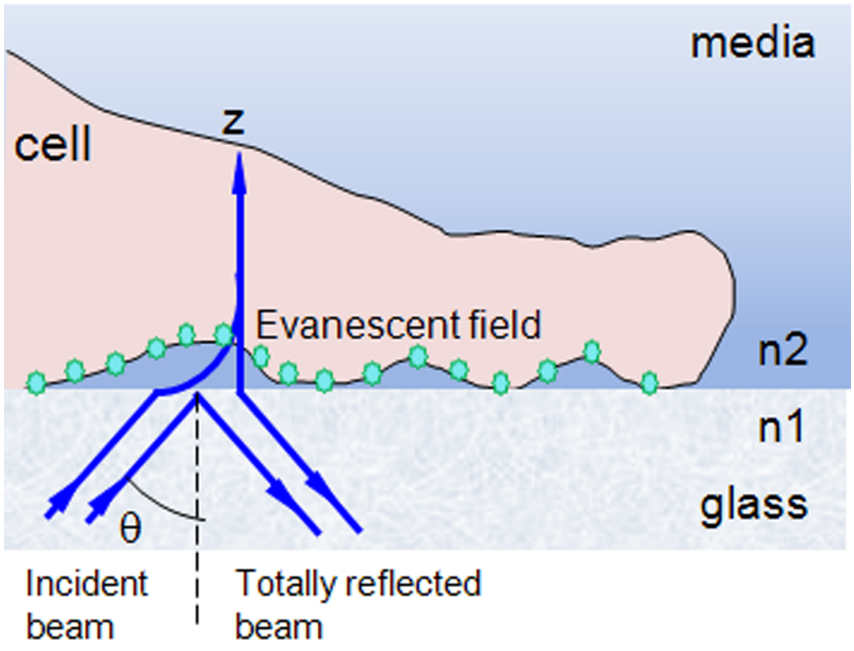

Figure 13: Schematic representation of the TIR effect.
The exponentially decreasing evanescent field enables selective excitation of the fluorophores at the cell-coverslip interface. (Adapted from Trache and Meininger, 2008b).

The relationship between the angle of incidence (θ_1) and refraction (θ_2) within mediums of different refractive indices (n_1, n_2) is governed by Snell's law;

$$n_1 \sin\theta_1 = n_2 \sin\theta_2 \quad (4)$$

The critical angle (θ_C) represents the angle of incidence when the refracted light propagates at the interface of the two media i.e., when $\theta_2 = 90°$ and is given by

$$\theta_C = \sin^{-1}\left(\frac{n_2}{n_1}\right) \tag{5}$$

When the angle of incidence is greater than the critical angle ($\theta_1 > \theta_C$) all of the incident light is reflected back into the high refractive media (n_1). The evanescent wave generated at the interface propagates into the lower refractive media (n_2). The maximum angle (θ_{Max}) the beam can emerge into the objective is given by

$$\theta_{max} = \sin^{-1}\left(\frac{NA}{n_1}\right) \tag{6}$$

where, NA is the numerical aperture of the objective.

The intensity of the evanescent field $I(z)$ decreases exponentially with the distance z from the interface of the two media, depending on both the incident angle and the polarization of the incident light and is given by

$$I(z) = I_0^{-z/d} \tag{7}$$

For a given incident light wavelength λ, d is the depth of field where the intensity of the evanescent light is $1/e$ of the boundary intensity, which is given by

$$d = \frac{\lambda}{4\pi}\frac{1}{\sqrt{n_1^2 \sin\theta_1^2 - n_2^2}} \tag{8}$$

This exponential decay of evanescent wave with distance from the interface confines the useful depth of penetration to about 100 nm into the sample (i.e., the practical distance

up to which the evanescent wave has enough energy to excite the fluorophores). Thus, TIRF microscopy provides high contrast images due to very low background. However, these high-contrast details are limited only to the basal cell surface, which is closest to the coverslip. Therefore, TIRF is an excellent technique to study focal adhesion of adherent cells as it enables quantitative measurements and localization of focal adhesion proteins that are important signaling centers between the cell and the external microenvironment (Axelrod, 2003; Trache and Meininger, 2008b).

3.1.3.2 TIRF configuration

Various optical configurations can be used to achieve TIRF in the optical microscope (Axelrod, 2001a; Axelrod, 2001b). We use the TIRF through-the-objective on an inverted microscope configuration as shown in Figure 14.

The laser beam used for excitation is focused at the back focal plane of the objective to collimate the beam and illuminate the sample at an angle of incidence θ with respect to the optical axis. A micrometer is used to move the optic fiber position with respect to optical axis such that the off-axis radial distance (δ) is increased to achieve supercritical incidence angle (i.e. $\theta_1 > \theta_C$) required for TIR (Trache and Meininger, 2008b). There is a one-to-one correspondence between the off-axis radial distance (δ), and the angle of incidence θ.

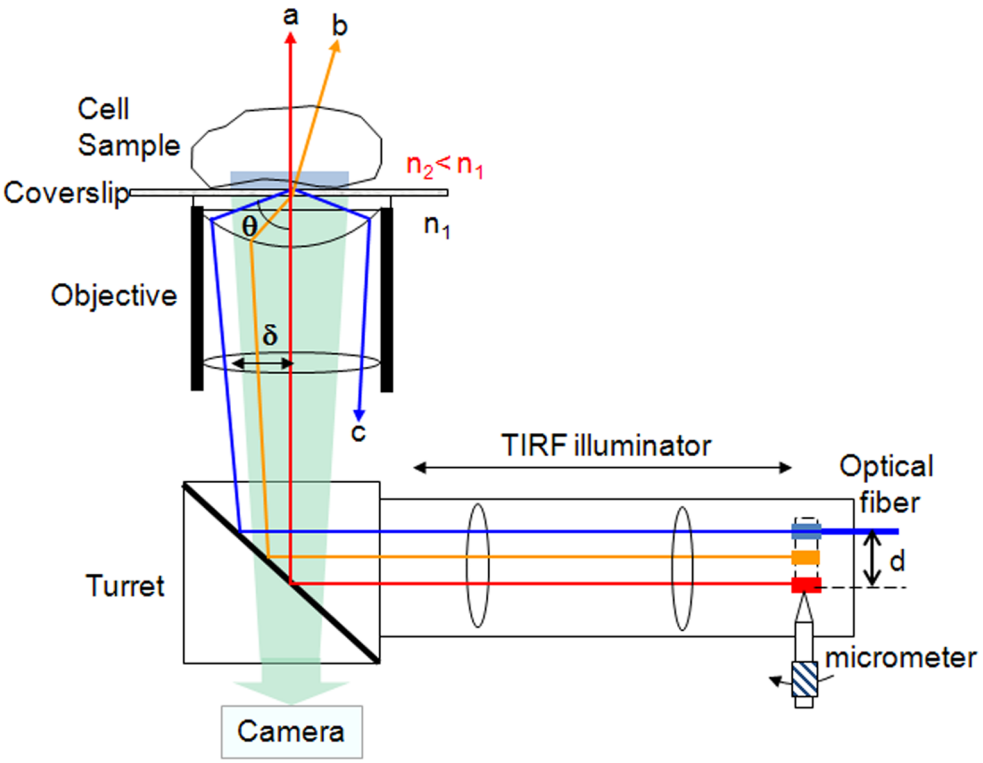

Figure 14: Schematic of TIRF optical path in the through-the-lens microscope configuration.
Ray a is obtained with the fiber optic centered on the optical axis. Ray b is obtained for an incident angle at the sample plane smaller than the critical angle. Ray c is obtained when TIR effect takes place. The fluorescence light reflected from the sample plane is collected through the same microscope objective and is further sent to the camera where the image is recorded. θ, angle of incidence at the sample; d, distance between the optical axis and the fiber position; δ, off-axis distance of the laser beam in the back focal plane of the objective. (Adapted from Trache and Meininger, 2008b)

3.1.4 Spinning disk confocal microscopy

Confocal microscopy is an optical microscopy technique that increases image contrast through spatial filtering. In conventional confocal microscopy, the sample is illuminated

point-by-point while a pinhole is used in front of the detector to collect only the photons emitted from the plane of focus while rejecting all out-of-focus light (Hibbs, 2004). This technique enables not only imaging of a very thin section of the sample but also optical sectioning of the sample along the axial direction, providing a 3-dimensional view of the sample. In contrast, spinning disk confocal microscopy illuminates and scans multiple points simultaneously to generate a 2D image of the sample plane in focus, enabling rapid optical sectioning of the sample in z-axis.

3.1.4.1 Principle of operation

Spinning disk confocal uses a dual-disk scanning system, composed of a pinhole disk (50 μm pinhole size) and a Fresnel micro-lens disk perfectly aligned such that each lens focuses the light through the corresponding pinhole as shown in Figure 15. Both disks follow the Nipkow disk pattern with 20,000 pinholes arranged in an interleaved spiral configuration with a constant 250 μm pitch for array scanning. The laser beam passes through the tandem-spinning dual disk to simultaneously illuminate the sample with 1000 beamlets (Graf et al., 2005; Inoué and Inoué, 2002; Kino, 1995). The fluorescence emitted from the sample passes through the same pinholes to spatially filter out all the out-of-focus light and then reaches the detector through a dichroic mirror placed between the disks. Due to the spiral pinhole pattern, every single position in the field of view is covered within 1/12th of one disk rotation. Therefore, if the disk rotates at a speed of 5000 rpm that translates to ~1000 full frames/second (Graf et al., 2005).

However, the speed of image acquisition is limited by the charged-coupled device (CCD) camera used as the imaging detector.

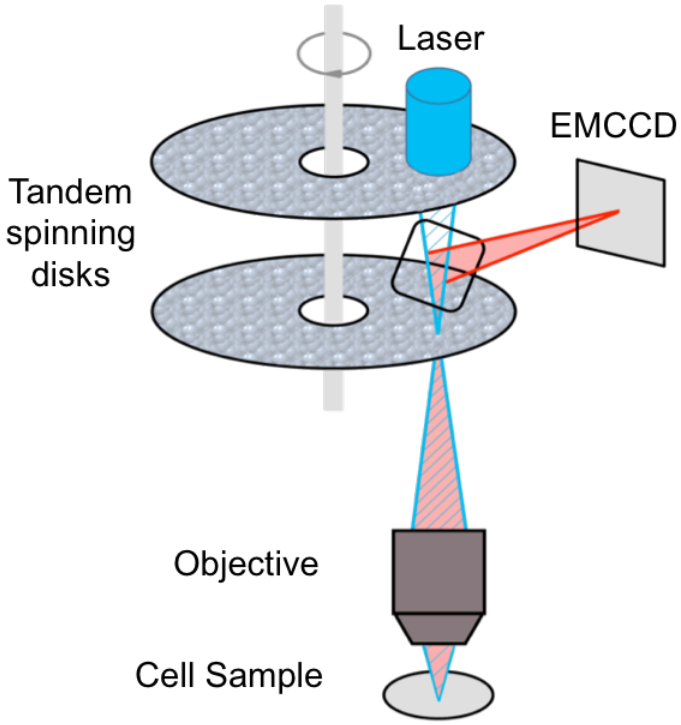

Figure 15: Schematic representation of the confocal optical path.

The CCD camera consists of a two-dimensional array of light-sensitive regions that convert the incident light intensity into an electric charge (Pawley, 2006). The electric charge is further digitized, reconstructed, and displayed on a computer screen enabling fast capture of the scanned data. Thus the camera exposure time and the frame readout speed limit the imaging speed that can be attained with the spinning disk device.

The spinning-disk confocal microscopy improvement in speed of acquisition greatly reduces photobleaching and phototoxicity, thus facilitating imaging of protein dynamics over extended periods of time (Graf et al., 2005). These properties make this technique suitable to study cytoskeletal dynamics with high spatial and temporal resolution.

3.2 Experimental Configuration of the Integrated Microscope System

In the studies presented, we used a Bioscope SZ AFM (Bruker Nano Surfaces, Santa Barbara, CA) mounted on top of an inverted Olympus IX-81 microscope integrated with a total internal reflection fluorescence (TIRF) attachment (Olympus, Center Valley, PA), CSU-22 Yokogawa spinning-disk confocal scanning head (Yokogawa Electric Inc., Japan) and QuantEM 512SC camera (Roper Scientific Photometrics, Tucson, AZ)

Our experiments were performed using the experimental parameters presented below. A PLAN APO 60x oil 1.45 NA TIRF objective lens was used for imaging live cells expressing fluorescent protein constructs. For TIRF, given the refractive index of oil is 1.516 and NA of 1.45; then, for wavelength of 488nm, one can calculate critical angle θ_C=61.4°, θ_{Max}=72.78° and a useful depth of field d ~ 92nm. 3D confocal images were acquired as stacks of 20 planes at a 0.25 μm step size, and are presented as xy projections. Both TIRF and confocal images were acquired with an exposure time of 100 ms.

To obtain AFM images of single live VSMC in culture, the AFM was operated under fluid in contact mode (Trache and Meininger, 2008a). The maximum scanned image size was 100 × 100 μm with a scan speed of 40 μm/s.

For adhesion force spectroscopy measurements, the AFM was operated in force mode. AFM probes functionalized with fibronectin were driven to touch and retract from the cell surface over 800 nm in the z-axis with a frequency of 0.5 Hz. The measurements were performed in a region midway between the nucleus and the edge of the cell. Data were acquired for 2 min per cell and repeated for 10 cells per dish, for 4-6 different dishes per condition, generating ~ 2,000-4,000 individual measurements for each case.

4 EXPERIMENTAL RESULTS*

4.1 Selective Regulation of Cellular Remodeling by RhoA and Src

Cardiovascular diseases such as hypertension and atherosclerosis are associated with increased vascular resistance due to vessel wall remodeling (Hayashi and Naiki, 2009; Intengan and Schiffrin, 2000; Pries et al, 2005;). Remodeling of the cytoskeleton and cell–matrix adhesions enable VSMC to sense and adapt to external mechanical stresses (Goldschmidt et al., 2001; Gunst and Zhang, 2008; Pries et al., 2005). Alteration in VSMC migration, proliferation, and contractility contributes to vessel wall remodeling (Gunst and Zhang, 2008; Ingber, 2002; Martinez-Lemus et al., 2009) resulting in arterial wall dysfunction.

Integrin-mediated cell–matrix adhesions trigger cytoskeletal changes that drive adaptive cellular responses, thus enabling vasculature function (Zhang and Gunst, 2006). Specifically, binding of matrix to integrin $\alpha_5\beta_1$ plays an important role in vascular contraction in response to increased pressure (Mogford et al., 1997; Wu et al., 2001; Martinez-Lemus et al., 2004). Src is a non-receptor tyrosine kinase belonging to Src family kinase (SFK), and is known to regulate the turnover of adhesion structures and

* Text reproduced with permission of The Royal Society of Chemistry (RSC) from Sreenivasappa et al., 2014, doi: 10.1039/c4ib00019f. Parts of this section are reproduced with permission of The Royal Society of Chemistry from Lim et al., 2012, doi: 10.1039/c2ib20008b. Parts of this section are reproduced from Papke CL et al., 2013, Human Molecular Genetics, with permission of Oxford publication, doi:10.1093/hmg/ddt167. Parts of this section are reproduced with permission from Journal of Cell Science, Chaki et al., 2013, doi: 10.1242/jcs.119610

cytoskeletal–integrin interactions through phosphorylation of focal adhesion associated proteins (Felsenfeld et al., 1999; Li and Xu, 2000). Signaling induced by integrin-dependent activation of Src is transferred to distant sites through cytoskeletal signaling (Wang et al., 2005). Activation of integrin $\alpha_5\beta_1$ is also associated with RhoA-mediated actomyosin contractility and increased cytoskeletal tension (Danen et al., 2005; White et al., 2007). Moreover, integrin $\alpha_5\beta_1$ adhesion to fibronectin is modulated by the Src–FAK complex (Ballestrem et al., 2006; Volberg et al., 2001), and Src stimulated adhesion turnover involves modulation of RhoA activity (Huveneers and Danen, 2009). Force application through functional FA along the fibronectin-integrin-actin axis induces adaptive cellular responses, including increased stress fiber remodeling and adhesion strength (Lim et al., 2012; Sun et al., 2008). However, the characteristics of the crosstalk between Src and RhoA and their relative contribution to tensional homeostasis and cell–matrix adhesion dynamics are poorly understood. To test the hypothesis that cell adhesion to the matrix is modulated by cytoskeletal tension through the crosstalk between RhoA and Src, we combined molecular approaches with fluorescence imaging and atomic force microscopy (AFM). This strategy enabled us to correlate structural cytoskeletal changes with functional $\alpha_5\beta_1$ integrin–fibronectin adhesion forces. Results suggest that $\alpha_5\beta_1$ integrin–fibronectin adhesion strength is regulated by cytoskeletal tension through a mechanism that involves modulation of downstream effectors of RhoA by Src.

4.1.1 The architecture of the actin cytoskeleton is differentially modulated by RhoA and Src

Stress fibers play a critical role in maintaining cell shape and tissue organization by transmission of tension and generation of force (Zhou and Liao, 2009). Activation of the RhoA pathway is a major mechanism promoting the assembly of stress fibers (Mack et al., 2001; Worth et al., 2004), and hence increased cytoskeletal tension (Lim et al., 2010; Lim et al., 2012). In addition, actin stress fiber morphology is directly linked to the formation and turnover of FA. To determine if there exists reciprocity between RhoA and Src in the regulation of the mechanosensitive apparatus consisting of stress fibers and associated FA, we performed confocal imaging of VSMC expressing the corresponding wild-type or mutant variants of these signaling molecules. As shown in Figure 16A, stress fiber morphology of cells expressing dominant negative (DN), wild type (wt), or constitutively active (CA) RhoA varied from almost unnoticeable, to well organized, to highly prominent, respectively. Consistent with previous findings (Lim et al., 2012), where some peripheral actin fibers were present, the majority of stress fibers disassembled in the center of cells expressing RhoA-DN. In contrast, a similarly organized arrangement of stress fibers was always present regardless of the c-Src variant expression. Quantitative analysis showed that the assembly of stress fibers increased significantly with RhoA activation, while a very modest increase was measured for c-Src activation (Figure 16B). These results suggest that in contrast to major reorganization of the actin network induced by RhoA modulation, only minor changes occurred in response to c-Src activation.

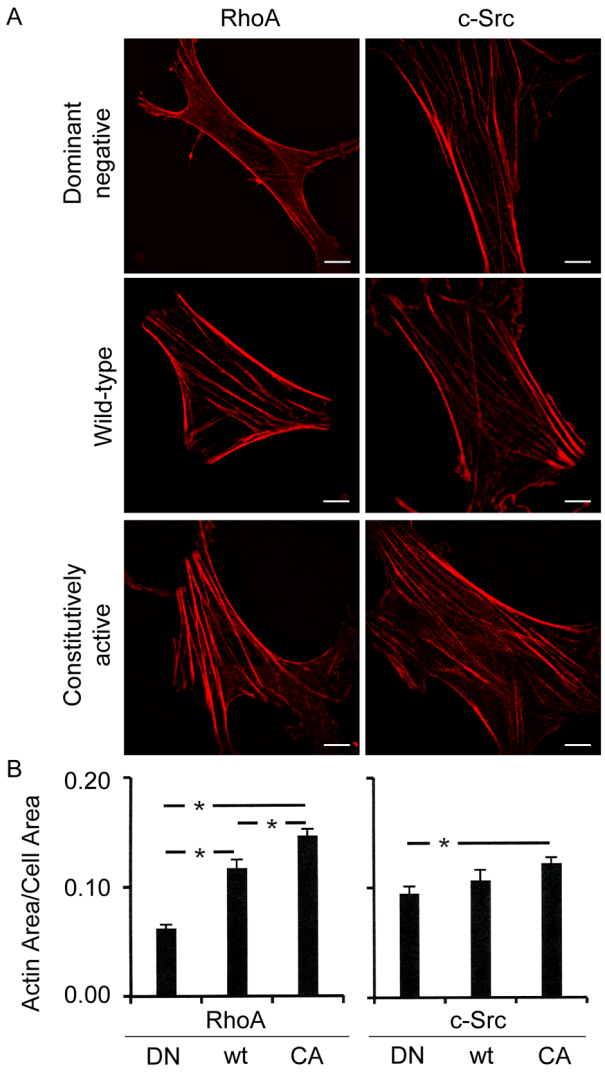

Figure 16: The architecture of the actin cytoskeleton is differentially modulated by RhoA and c-Src.
(A) Representative confocal images of VSMC co-expressing actin-mRFP and wild type (wt)/mutant versions (DN – dominant negative, CA – constitutively active) of RhoA-EGFP or c-Src-EGFP are shown (green channel not shown for clarity). RhoA activation increases formation of stress fibers, while its inhibition downregulates fiber formation mainly in the cell body, preserving the actin bundles at the cell edges. c-Src activation has only a modest effect on the morphology of actin stress fibers. Scale bar represents 10μm. (B) Quantitative analysis of actin remodeling (n >6) induced by expression of wt/mutant versions of RhoA-EGFP or c-Src-EGFP (mean ± SE). Significance was evaluated at $p < 0.05$ (Reproduced with permission of The Royal Society of Chemistry (RSC) from Sreenivasappa et al., 2014, doi: 10.1039/c4ib00019f).

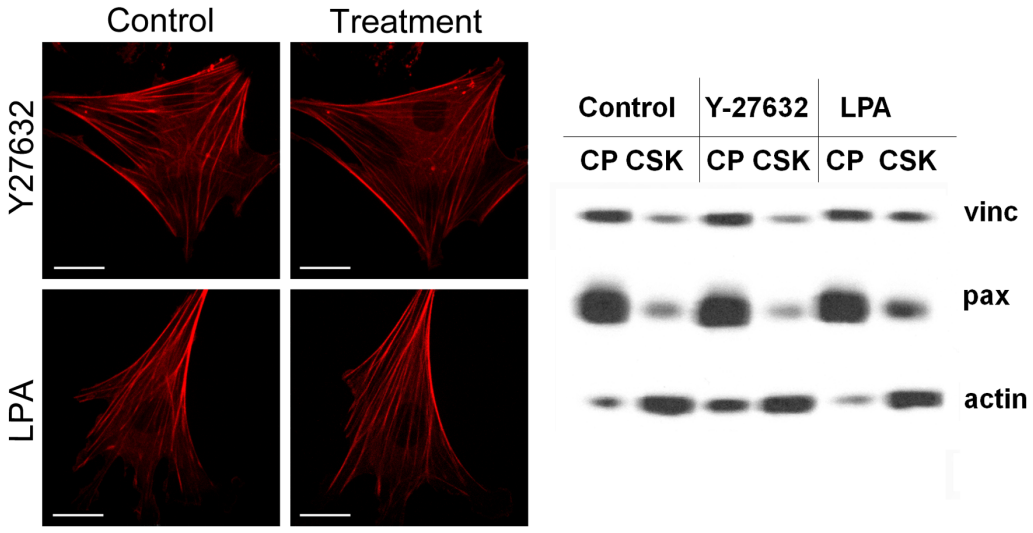

Figure 17: Effects of Y-27632 and LPA treatments on VSMC.
VSMC expressing actin-mRFP before (control) and after treatment with Y-27632 or LPA is shown together with western blot analysis performed for cytoplasmic (CP) and cytoskeletal (CSK) fractions. Antibodies specific to vinculin, paxillin, and actin were used. Scale bar represents 10μm. (Reprinted from Lim et al., 2010 with permission from Elsevier, doi:10.1016/j.yexcr.2010.06.010).

To independently test the RhoA effects on VSMC morphology, drug treatments were used to inactivate or activate the RhoA pathway. Treatment of VSMC with the Rho-Kinase inhibitor Y-27632 reduced the stress fibers in the center of the cell, but maintained peripheral stress fibers (Figure 17), phenocopying the RhoA-DN effect. These data are supported by western blot analysis showing that the relative amount of actin decreased by 22% in the cytoskeletal fraction in comparison with control (Lim et al., 2010). Treatment of VSMC with LPA induced stress fiber formation, phenocopying the RhoA-CA effect. The western blot analysis showed that the relative amount of actin increased by 46% in the cytoskeletal fraction in comparison with control. The

cytoskeletal fraction is representative for our imaging experiments, and the trend shown by the western blot analysis is consistent with our imaging data.

4.1.2 The architecture of focal adhesions is differentially modulated by RhoA and Src

Activation of RhoA also induces maturation of FA (Lim et al., 2010), a process reflected by the accumulation of tyrosine phosphorylated proteins at adhesion sites. Furthermore, integrin engagement recruits and activates a FAK/Src complex that promotes the assembly and maturation of cell-matrix adhesions (Huveneers et al., 2008; Volberg et al., 2001). Recent evidence suggests that impaired stress fiber assembly precludes maturation of FA (Gardel et al., 2010). Since there is extensive crosstalk between c-Src and RhoA in the regulation of cell-matrix adhesions (Huveneers and Danen, 2009), we compared the extent of FA assembly and maturation induced by RhoA vs. c-Src. Focal adhesion assembly, determined by TIRF imaging of cells expressing fluorescently tagged vinculin, was dependent on both RhoA (Figure 18A) and c-Src (Figure 18B) activation. Thus, vinculin recruitment at adhesion sites was low, intermediate, and high in cells expressing RhoA- or c-Src-DN, -wt, and -CA, respectively. We also determined the extent of adhesion maturation using dSH2-EYFP, a previously described reporter for tyrosine phosphorylation of focal adhesion-associated proteins (Kirchner et al., 2003). Adhesion maturation was dependent mainly on RhoA activation, as evidenced by the expression of RhoA-CA (Figure 18A) and the increase in the accumulation of tyrosine phosphorylation following activation of endogenous RhoA by LPA treatment (Figure 18C). In contrast, c-Src-induced adhesion maturation increased significantly with its

modulation.

To further assess the role of localized c-Src activation on adhesion maturation, we determined the subcellular distribution of the c-Src variants. C-Src-CA, but not c-Src-DN or -wt, localized predominantly to FA (Figure 19A), as previously shown by Kaplan et al. (Kaplan et al., 1994; Kaplan et al., 1995). The phosphotyrosine reporter dSH2 (Src homology 2 domain) and immunolabeling with an anti-phosphotyrosine antibody revealed that both peripheral and central FA contained tyrosine phosphorylated proteins (Figure 19B, top panel). The level of tyrosine phosphorylation at FA was significantly decreased by SU6656, a cell-permeable small molecule that specifically inhibits Src kinase with high affinity (Blake et al., 2000). Src-dependent FA maturation is demonstrated by the significant decrease of phosphotyrosine accumulations at FA in cells treated with SU6656, which also corresponded to a decrease in c-Src-CA localization to FA under the same treatment conditions (Figure 19B, lower panel).

Collectively, these results suggest that non-redundant cues from RhoA and c-Src regulate the organization and signaling of the cell's mechanosensitive system consisting of stress fibers and associated FA.

Figure 18: RhoA and c-Src differentially regulate focal adhesion organization and activation.
Representative TIRF images of VSMC co-expressing fluorescently-tagged vinculin or dSH2 and RhoA (A) or c-Src (B) variants are shown. Vinculin was used to report the overall FA morphology, while dSH2 was used to report tyrosine phosphorylation. (C) Representative TIRF images of VSMC expressing dSH2-EYFP untreated (Ctrl) or treated with LPA. Scale bar represents10 μm. Quantitative measurements ($n > 6$) are presented as mean ± SE. Significance was evaluated at $p < 0.05$ (Reproduced with permission of The Royal Society of Chemistry (RSC) from Sreenivasappa et al., 2014, doi: 10.1039/c4ib00019f).

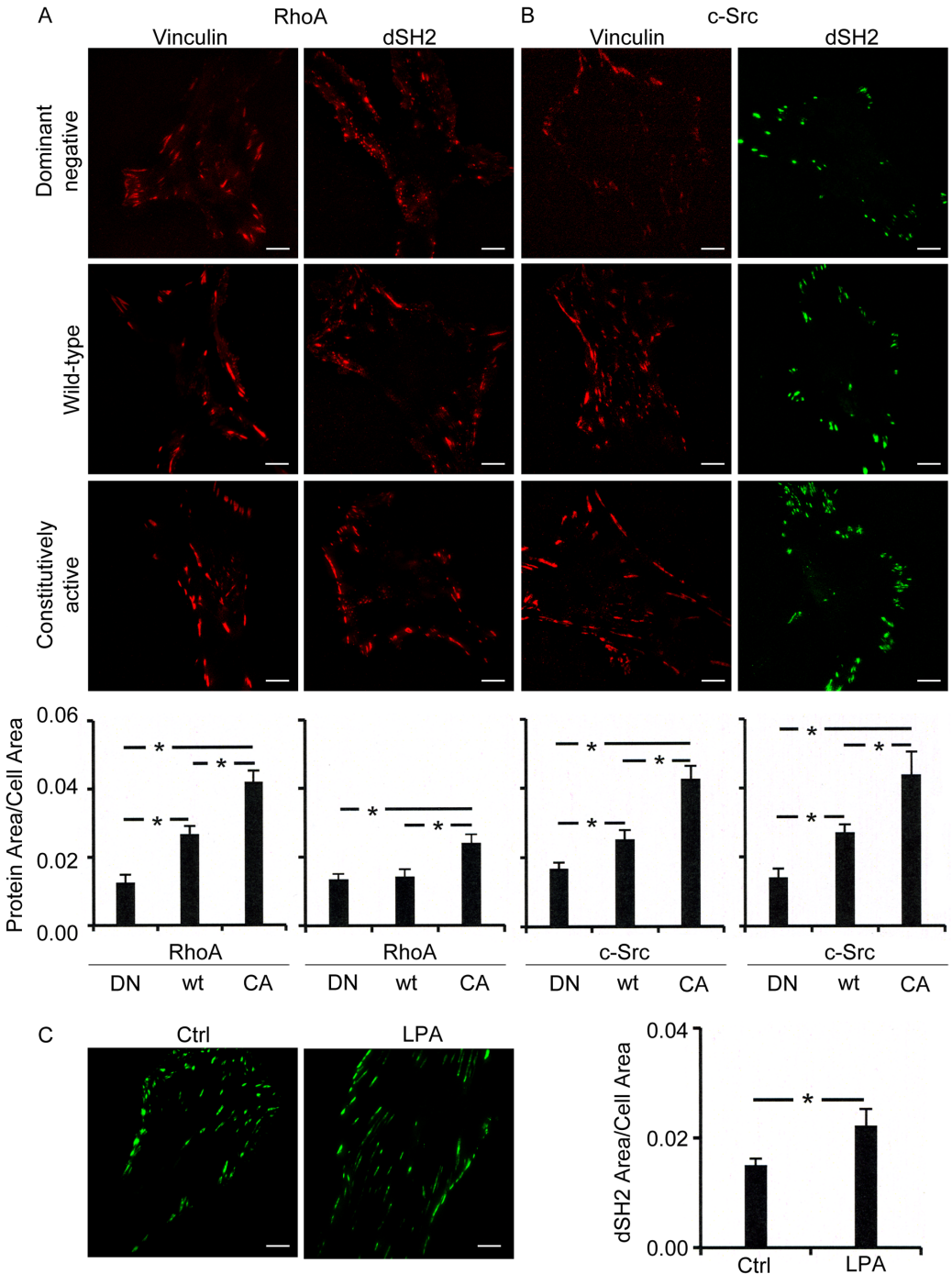
A
RhoA
Vinculin
dSH2
B
c-Src
Vinculin
dSH2
Dominant negative
Wild-type
Constitutively active
Protein Area/Cell Area
0.06
0.04
0.02
0.00
RhoA
RhoA
c-Src
c-Src
DN
wt
CA
C
Ctrl
LPA
dSH2 Area/Cell Area
0.04
0.02
0.00
Ctrl
LPA

Figure 19: Effect of c-Src inhibition on FA formation.
(A) Representative fluorescence images of wt/mutant versions of c-Src-EGFP. Constitutively active mutation of Src Y527F induces redistribution of c-Src from the cytoplasmic compartment to peripheral FA. (B) Representative TIRF images of control and SU6656 treated cells. Relative measurements of protein area show that after SU6656 treatment: (i) c-Src-CA expressing cells show 30% delocalization of c-Src-CA away from FA; and (ii) SH2 specific FA protein phosphorylation as well as total tyrosine phosphorylation at FA (immunofluorescence staining for pTyr antibody) is significantly reduced. Data are presented as mean ± SE. Significance was evaluated at $p < 0.05$ (Reproduced with permission of The Royal Society of Chemistry (RSC) from Sreenivasappa et al., 2014, doi: 10.1039/c4ib00019f).

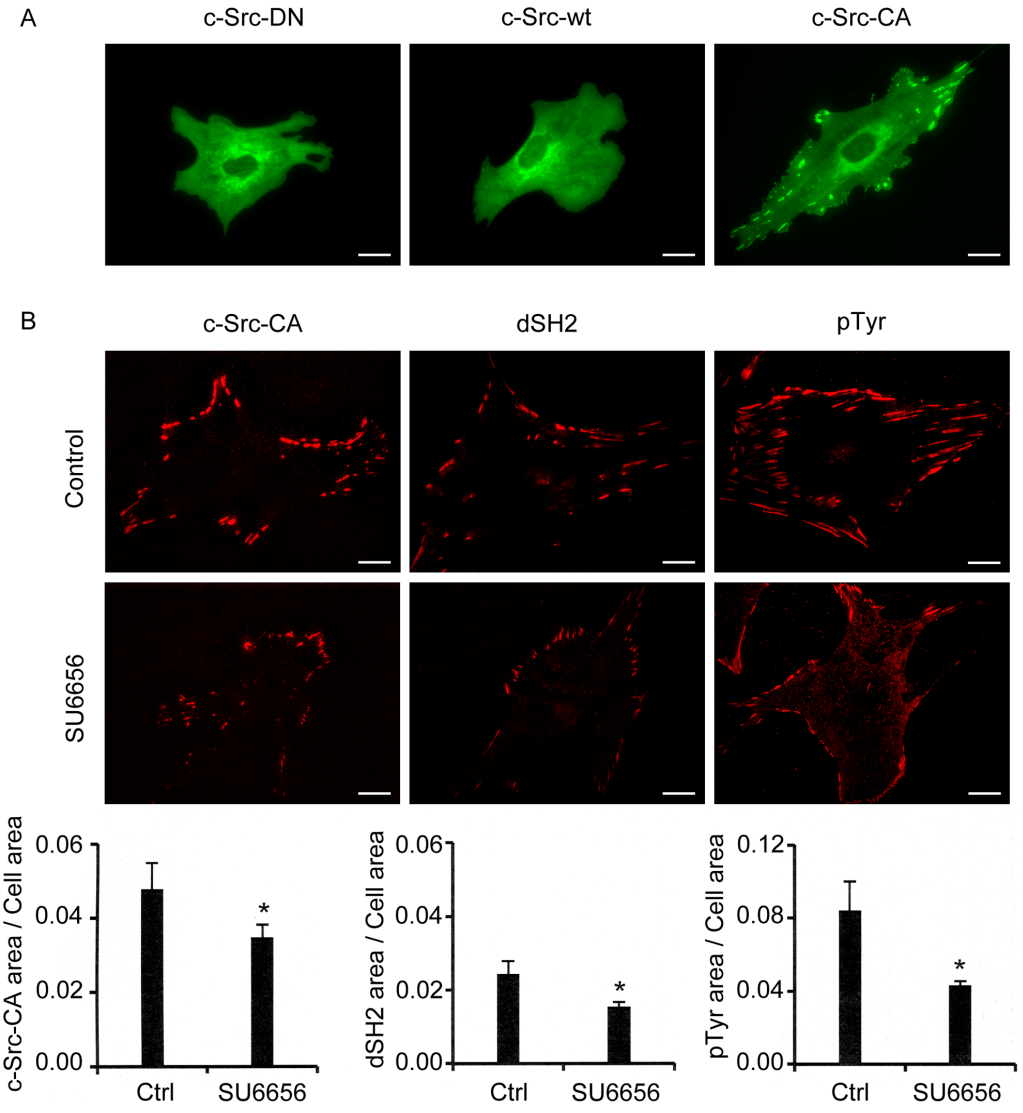
A
c-Src-DN
c-Src-wt
c-Src-CA
B
c-Src-CA
dSH2
pTyr
Control
SU6656
c-Src-CA area / Cell area
0.06
0.04
0.02
0.00
Ctrl
SU6656
*
dSH2 area / Cell area
0.06
0.04
0.02
0.00
Ctrl
SU6656
*
pTyr area / Cell area
0.12
0.08
0.04
0.00
Ctrl
SU6656
*

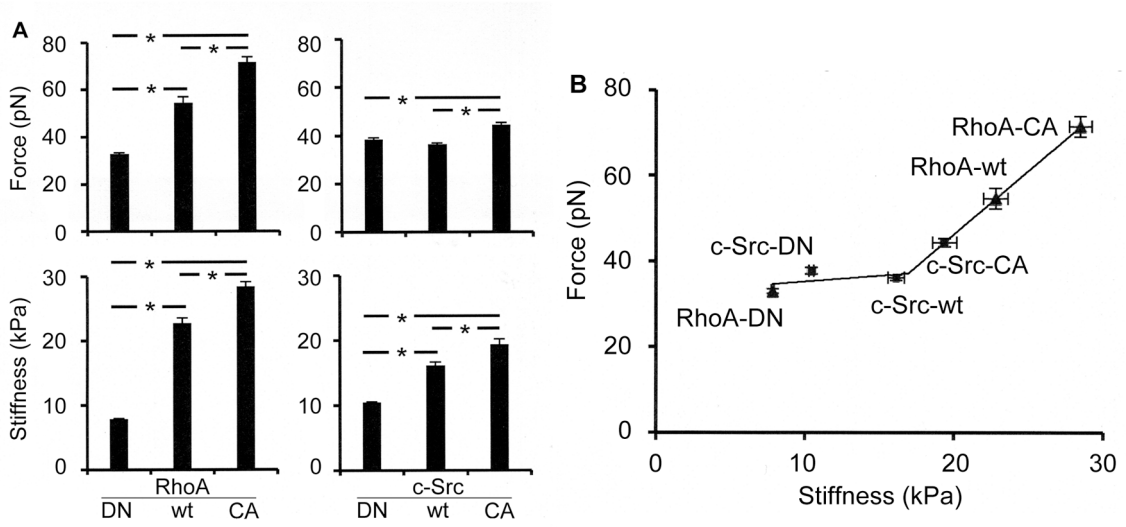

Figure 20: Integrin $\alpha_5\beta_1$-fibronectin adhesion force spectroscopy measurements. (A) Cell stiffness and adhesion force measurements were performed on cells expressing RhoA or c-Src variants. Cell stiffness significantly increased with both RhoA and c-Src activation, but the cell stiffness variation was more pronounced in RhoA- than in c-Src-expressing cells. The adhesion force of integrin $\alpha_5\beta_1$ binding to fibronectin progressively increased with RhoA activity. Downregulation of c-Src had no effect on integrin binding, while c-Src-upregulation induced an increase in adhesion strength. (B) Piecewise fitting of the force-stiffness experimental data shows two functional regimes for $\alpha_5\beta_1$ integrin binding to fibronectin: a slow change in stiffness but not in adhesion strength (slope = 0.27) up to a threshold stiffness of ~ 17 kPa (corresponding to an adhesion force of ~ 37 pN), followed by a rapid change (slope = 2.98) in both cell stiffness and adhesion force above the threshold. Data are presented as mean ± SE. Significance was evaluated at $p < 0.05$. (Reproduced with permission of The Royal Society of Chemistry (RSC) from Sreenivasappa et al., 2014, doi: 10.1039/c4ib00019f).

4.1.3 Differential modulation of cytoskeletal tension by RhoA and Src alters the functional coupling between adhesion force and cell stiffness

Based on the extensive cytoskeletal remodeling induced by activation of RhoA but not Src, we hypothesized that differences in cytoskeletal tension would be linked to a tightly coupled adhesion force-stiffness relationship in cells expressing RhoA but not c-Src

variants. To test this hypothesis, we measured cell stiffness and single ligand-integrin $\alpha_5\beta_1$ adhesion forces using an AFM probe functionalized with fibronectin. Cell stiffness is linked to the physical and functional integrity of the actin cytoskeleton and, therefore is considered a measure of cytoskeletal tension (Lim et al., 2012). Cell stiffness significantly increased with both RhoA and c-Src activity; however, the incremental change in cell stiffness was more pronounced in RhoA- than in c-Src-expressing cells (Figure 20A). This finding is consistent with major cytoskeletal remodeling accompanying RhoA but not c-Src activation.

In addition, adhesion strength presented different characteristics depending on the pre-stress level induced by the cytoskeletal tension (i.e., cell stiffness) (Figure 20B). Adhesion force of $\alpha_5\beta_1$ integrin to fibronectin directly increased with RhoA activity, while expression of c-Src-CA induced only a modest increase in adhesion force. The force-stiffness experimental data were modeled with a piecewise algorithm in which the data were fitted with two separate equations representing two straight line segments joined at their intersection point. The coordinates of the intersection point were selected in an iterative process to provide the best overall fit to the data (Muggeo, 2003). This data fitting was performed using piecewise continuous functions in SigmaPlot 9.0 (*Systat Software Inc*., Chicago, IL). The lower segment presented almost a flat dependence (slope 0.27) of force vs. stiffness, while the upper segment presented a rapidly increasing positive dependence (slope 2.98). The intersection coordinates provided a stiffness threshold corresponding to ~ 17 kPa, below which the integrin-FN

adhesion force is ~ 37 pN without significant variations. However, above this threshold the force increases rapidly with the increase in cell stiffness. Thus, soft cells exhibiting a cytoskeletal tension below the threshold value present no significant variation in the adhesion force to the matrix, while stiffer cells exhibiting a cytoskeletal tension above the threshold present a significant increase in adhesion strength, presumably through a mechanism that involves integrin activation.

Taken together, these results suggest that RhoA and c-Src activation have different effects on cytoskeletal tension development, inducing two distinct force-stiffness functional regimes for $\alpha_5\beta_1$-integrin binding to fibronectin.

4.1.4 Actomyosin apparatus coordinates the ability of cells to adapt to the external force

Given the differential regulation of cytoskeletal tension between RhoA and c-Src, we further investigated the implications of actomyosin apparatus in cytoskeletal tension development. The cellular response to mechanical stimulation is a balance between contractile elements in the actomyosin apparatus and FA (Romer et al., 2006; Wolfenson et al., 2011). Figure 21A shows that AFM mechanical stimulation at the apical cell surface induces significantly different cell responses that depend on cytoskeletal tension and myosin function. To assess the adaptive response of VSMC to external tensile stress for each treatment, the overall displacement was plotted as a function of time for the duration of the experiment. For cells expressing RhoA-DN, the AFM probe detaches

from the cell surface at the first mechanical stimulation with 1 nN force, and the overall curve exhibits a linear dependence.

Despite the short duration for this set of experiments, the displacement was maximal. In the absence of cortical actin fibers, cells are soft, the FA formed between the cell and the FN coated bead is weak, and the myosin has no ability to act in the absence of the actin network. The ultimate result is poor cell contractility and the loss of contact between the AFM probe and the cell. RhoA-CA expressing cells were found to exhibit high contractile activity due to strong actin fibers formation, but at the same time they were also elastic and able to pull back after initial tensile force application. The overall displacement exhibited a high reactive response with time. In contrast, cells treated with ML-7, a potent smooth muscle myosin inhibitor, were significantly softer (12.1 ± 2.8 kPa) than RhoA-CA expressing cells and the overall dependence plateaued at high force values. Thus, myosin blocking induced a decrease in cellular contractility. In addition, Figure 21B shows representative confocal images of cells expressing actin-mRFP treated with ML-7 in comparison with control (i.e., no drug treatment). ML-7 suppressed the formation of strong actin fibers at cell edges (white arrow heads), demonstrating the role of myosin in actin fiber formation and maintenance of cytoskeletal tension.

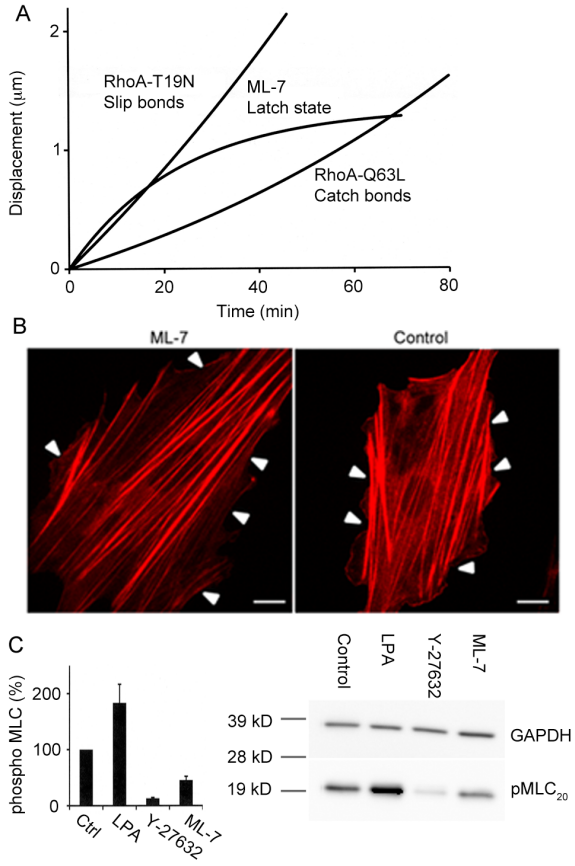

Figure 21: Cell responses to mechanical stimulation depends on cytoskeletal tension and myosin function
(A) Overall displacements for each treatment were compiled over the duration of the mechanical stimulation experiment. Cellular adaptive response to force is modulated by the cytoskeletal tension, which in turn is dictated by the treatments applied to the cell. Cells expressing RhoA-T19N (DN) detach from the FN-probe at the first mechanical stimulation with 1 nN force, and the overall curve exhibits a linear dependence with a maximal displacement (slip bonds). RhoA-Q63L (CA) expressing cells were found to resist applied tensile stress and exhibit high contractility power, showing a reactive response to the applied stress (catch bonds). In contrast, cells treated with ML-7 display an overall dependence that plateaus at high force stimulation (latch state). (B) Representative confocal images show that ML-7 impedes formation of strong actin fibers at cell edges in comparison with control (see arrows). Scale bar is 10 μm. (C) Western blot quantitative densitometry analysis shows that MLC phosphorylation increased in LPA treated cells and decreased in cells subjected to Y-27632 or ML-7 treatments. Results presented as percent change in respect to control. (Reproduced by permission of The Royal Society of Chemistry from Lim et al., 2012, doi: 10.1039/c2ib20008b).

To independently verify the role of MLC phosphorylation in cytoskeletal tension modulation, western blots were performed on total cell lysates obtained from cells treated with LPA and Y-27632 (Figure 21C). MLC phosphorylation was increased in LPA treated cells and severely decreased in cells subjected to Y-27632 treatment (Lim et al., 2012). As expected, results showed that MLC phosphorylation is directly dependent on RhoA pathway activation. Also, as shown above, MLC phosphorylation decreased in cells treated with ML-7. Taken together, from these results we conclude that the integrity of the actin network coupled with myosin function is responsible for the ability of cells to respond and adapt to mechanical microenvironmental stimuli.

4.1.5 Src modulates cytoskeletal tension via RhoA crosstalk

Given the differential regulation of cytoskeletal tension and FA formation between RhoA and c-Src, we asked if the c-Src-induced cytoskeletal tension involved modulation of the RhoA pathway. To test this hypothesis, we determined the mechano-sensitive response to c-Src inhibition by using SU6656 in cells expressing RhoA-CA. As expected, RhoA-CA expression induced a significant increase of both cell stiffness and adhesion strength above control. However, SU6656 treatment abolished these effects by releasing RhoA-induced contractile cytoskeletal tension (Figure 22A). Following treatment with SU6656, the increase in $\alpha_5\beta_1$-FN adhesion force induced by RhoA-CA expression was significantly lowered to levels comparable to those measured in control cells under the same treatment, while stiffness was further decreased to levels measured in cells expressing RhoA-DN.

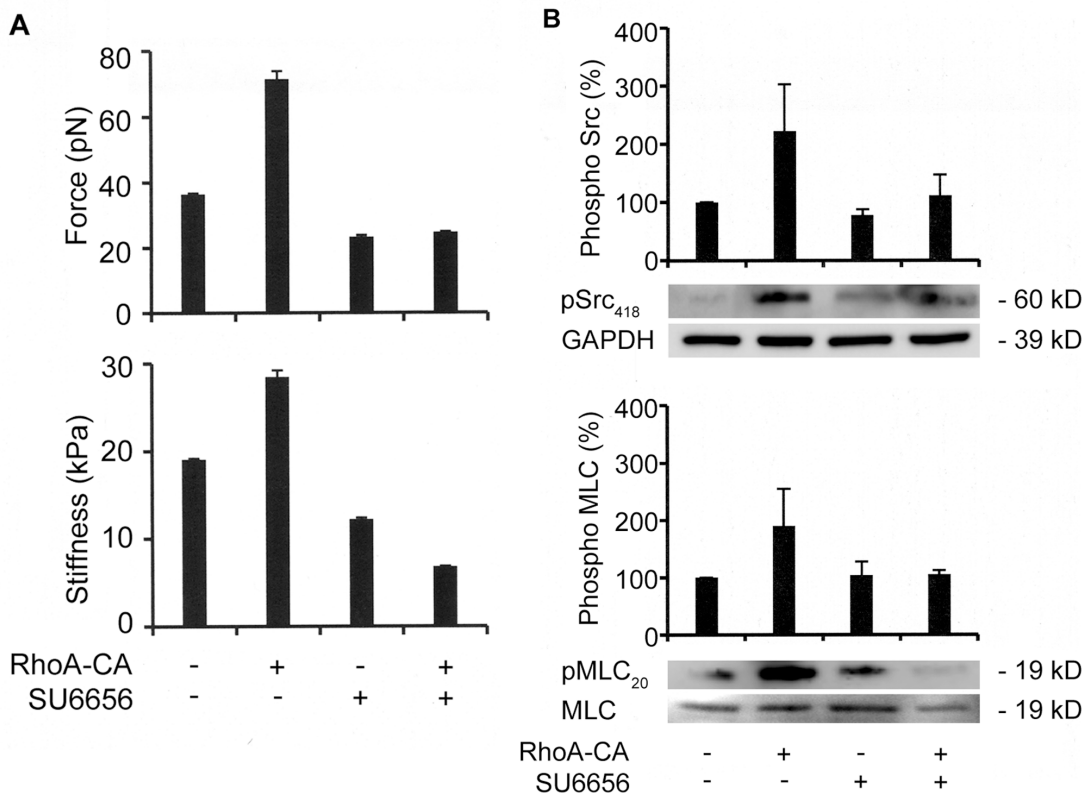

Figure 22: Src-dependent modulation of the RhoA pathway.
(A) Adhesion force spectroscopy measurements show that c-Src inhibition in control as well as RhoA-CA expressing cells significantly reduces $\alpha_5\beta_1$ integrin adhesion force and cell stiffness. Data are presented as mean ± SE. Significance was evaluated at $p < 0.05$. (B) Western blot quantitative densitometry analysis shows that Src Y418 and MLC phosphorylation decrease in RhoA-CA expressing cells treated with Src inhibitor SU6656. Results are presented as percent change in respect to control (Reproduced with permission of The Royal Society of Chemistry (RSC) from Sreenivasappa et al., 2014, doi: 10.1039/c4ib00019f).

The present results show a progressive increase in cell stiffness in response to RhoA activation and, to a lesser extent, c-Src activation. These findings prompted us to test if Src contributes to the modulation of myosin, a RhoA downstream effector. Thus, cells

expressing RhoA-CA and further treated with SU6656 Src inhibitor showed decreased c-Src and MLC phosphorylation (Figure 22B). Taken together, these results suggest that c-Src modulates the RhoA pathway through direct modulation of downstream effectors.

4.1.6 Discussion

This study used a combination of single ligand-receptor interaction measurements and fluorescence imaging on live cells to analyze the relationship between cytoskeletal tension and integrin $\alpha_5\beta_1$ adhesion strength to fibronectin in response to combinatorial signaling from RhoA and c-Src. The present study shows that: (i) $\alpha_5\beta_1$ integrin binding to the matrix presents two distinct functional regimes dependent on the cytoskeletal tension induced by RhoA and c-Src activation, (ii) pre-existing cytoskeletal tension induced by RhoA activation directly affects the actomyosin apparatus that modulates the ability of VSMC to adapt to the applied force, and (iii) Src induces cytoskeletal tension modulation via cross-talk with the RhoA pathway.

The mechanotransduction process involves tension-dependent conformational changes of key mechanosensory and signaling FA proteins, as well as activation of RhoA that functions as a molecular switch to induce actin and FA remodeling (Huveneers and Danen, 2009). The specialized smooth muscle cell contractile unit enables the cell to contract and relax through cyclic interactions between actin and myosin filaments regulated specifically by MLC kinase and phosphatase, respectively (Hong et al., 2011).

The regulation of cytoskeletal tension and adhesion dynamics through c-Src and RhoA

plays a central role in cellular adaptive responses as a result of integrin activation. c-Src, a non-receptor tyrosine kinase, is implicated in VSMC adhesion and contraction (Janssen et al., 2001; Ohanian et al., 1997). RhoA-mediated cytoskeletal tension induces an increase in cellular contractility and $\alpha_5\beta_1$ integrin-fibronectin adhesion strength (Huveneers and Danen, 2009; Lim et al., 2012). We have shown that integrin $\alpha_5\beta_1$ is the main mechanosensor (Lim et al., 2012) able to induce sustained mechanical stimulation under external force application through fibronectin functionalized AFM probes in VSMC (Lim et al., 2012). The activated β_1 integrin cytoplasmic tail provides binding sites for the Src-homology-2 domain (dSH2) of Src and mediate FAK Y397 phosphorylation (Arias-Salgado et al., 2003). This FAK-Src complex activity is important for cell spreading and adhesion (Ballestrem et al., 2006; Volberg et al., 2001), being part of the signaling pathway downstream of integrin-matrix interactions. Furthermore, c-Src has an important role in the crosstalk with the RhoA pathway by controlling guanine-exchange factors (Huveneers and Danen, 2009; Knock et al., 2008), and may modulate Rho-kinase induced force generation (Knock et al., 2008; Nakao et al., 2002). Rho-kinase activation downstream of RhoA increases cytoskeletal tension, which in turn has a robust effect on adhesion strength and integrin binding (Lim et al., 2012). Moreover, c-Src modulation of cell adhesion is involved in RhoA-mediated cytoskeletal contractility (Huveneers et al., 2007; Jiang et al., 2006).

Quantitative analysis has been performed on confocal and TIRF images of VSMC expressing RhoA and c-Src variants in order to determine morphological changes of

actin stress fibers and FA, respectively. In VSMC co-expressing actin-mRFP, RhoA-CA induced high cytoskeletal tension, measured by enhanced actin fiber formation and increased cell stiffness compared to cells expressing RhoA-wt. In contrast, RhoA-DN induced low cytoskeletal tension with actin bundles present only at cell edges (Lim et al., 2012), and a three-fold decrease in cell stiffness compared to RhoA-wt expressing cells. The results showed that in contrast with the RhoA effect on significantly modulating stress fiber formation, c-Src activation had only a modest effect on actin morphology. Drug treatments phenocopied mutant RhoA construct effects on VSMC contractility. Treatment of VSMC with Rho-kinase inhibitor Y-27632 (Katoh et al., 2001; Maekawa et al., 1999) reduced the number of stress fibers in the center of the cell, but maintained the peripheral stress fibers, phenocopying the effect of RhoA-DN. Loss of actin stress fibers from the cell body is in good agreement with our fluorescence imaging data in VSMC treated with RhoA-DN. In contrast, LPA treatment is known to modulate the mechanotransduction pathways (Ohata et al., 1997) inducing stress fiber and FA formation via activation of RhoA (Cerutis et al., 1997; Moolenaar, 1995). TIRF imaging showed that c-Src activation directly correlated with FA maturation by inducing protein recruitment and activation, while less emphasis was recorded for RhoA activation.

Single integrin $\alpha_5\beta_1$-fibronectin adhesion force measurements exhibited two distinct force-stiffness functional regimes for integrin $\alpha_5\beta_1$ binding to fibronectin. Cell stiffness measurements showed that cytoskeletal tension due to c-Src modulation varies to a

lesser extent in contrast with the progressive dependence of RhoA activation, which enabled a four-fold increase in cytoskeletal tension that induced a two-fold increase in adhesion strength to the matrix. Only expression of c-Src-CA increased cell stiffness above the threshold, which also induced an increase in adhesion strength.

Axial stress is a fundamental contributor to blood vessel wall homeostasis *in vivo*. The adaptive responses to altered loads in isolated arteries are compensated by a reduction in axial tension due to an increase in unloaded length (Humphrey et al., 2009). In order to study the axial stress effect on VSMC, external tensile stress was applied to cells presenting a pre-existing cytoskeletal tension modulated by RhoA activation. The VSMC contractility state is mainly determined by the MLC phosphorylation level, which enables myosin molecular interaction with actin (Amano et al., 1996; Amano et al., 1997; Kureishi et al., 1997). Blocking myosin function disrupts the formation of strong actin fibers at the cell edges, and induces a reduced cytoskeletal tension measured by low cell stiffness. Increased MLC phosphorylation induces generation of contractile force via an increase in the ATP activity of myosin II (Kaunas and Deguchi, 2011; Sugita et al., 2011) resulting in contraction of actin cytoskeleton due to increased crossbridge activity, while blocking of myosin activity by ML-7 results in reduced crossbridge kinetics. We suggest that ML-7 treated VSMC response to force represents the latch state, where the crossbridge cycling rates and MLC phosphorylation are low (Gunst and Fredberg, 2003; Murphy, 1994;). Under these conditions, all the elements of a functional FA are present, however, the contractility state of the actin cytoskeleton and

its ability to resist the applied force are reduced (i.e., overall displacement plateaus with time). This is consistent with Gunst et al. (Gunst et al., 2003) who showed that smooth muscle cells are able to maintain the tone and shape of hollow organs at a very low ATP metabolizing rate.

Force-sensitive changes under conditions of imposed stress are governed by actomyosin adaptation to the applied force, which is demonstrated by the direct dependence of cell stiffness on the cytoskeletal tension; this in turn correlates well with the presence of the stress fibers in the cell body. In order to understand cellular adaptive remodeling to external mechanical stimulation, the applied force must be exerted for a sufficient time to activate biochemical pathways that induce cytoskeletal remodeling by establishing a new homeostatic state. The strength of the FA directly determines the protein exchange rates within, and the degree of integrin activation. Ligand-receptor (i.e., ECM-integrin) interaction bonds have finite lifetimes that are dictated by the bond dissociation under applied force (Hoffman et al., 2011). In RhoA-DN expressing cells, the initial functional FA formed at the FN probe-cell interface was unable to strengthen enough with time due to the absence of a strong cortical actin, such that the integrin–ECM interactions in RhoA-DN expressing cells are characterized by slip-bonds (i.e., tensile stress shortens the ligand–receptor bond lifetime) (Evans and Calderwood, 2007). This type of interaction may explain the premature loss of contact with the FN functionalized probe, due to slip-bond breakage induced by the application of high forces. In contrast, in VSMC expressing RhoA-CA, FA strengthened with time, such that the integrin–ECM

interaction is characterized by catch-bonds (i.e., tensile stress strengthens the ligand–receptor bond) (Kong et al., 2009; Marshall et al., 2003; Thomas et al., 2008; Zhu and McEver, 2005). This type of interaction is possible due to reinforcing of the FA by recruiting actin, and activating linker and structural proteins that generate a long-lived interaction under tensile stress. The relative contributions of cellular structural components to intracellular force balance are ultimately determined by the cytoskeleton engagement to propagate the stimulation to distant sites and the strength of cell-matrix adhesions (Matthews et al., 2006).

Downregulation of c-Src had no major effect on $\alpha_5\beta_1$-FN adhesion strength, however, it decreased cytoskeletal tension through a cross-talk with RhoA pathway involving reduced MLC phosphorylation. This result is in agreement with previous findings by Felsenfeld et al. (Felsenfeld et al., 1999), which showed that loss of c-Src expression does not affect $\alpha_5\beta_1$ integrin-fibronectin interactions. We suggest that cytoskeletal tension regulation by c-Src activation is due to reinforcement and maturation of FA correlated with regulation of MLC activation, which is a downstream effector of the RhoA pathway. This finding is in agreement with Knock et al. (Knock et al., 2008), who showed MLC phosphorylation (Ser-19) downregulation by SU6656 on whole artery lysates. Although the mechanism underlying the lower cell stiffness measured in RhoA-CA-expressing cells following SU6656 treatment is not apparent, it is possible that cytoskeletal tension becomes more dependent on Src-regulated pathways under the expression of RhoA-CA. Thus, the interaction between RhoA activation and Src

deserves further investigation.

A possible mechanism by which c-Src-RhoA cross-talk modulates cytoskeletal tension, which in turn affects cell adhesion is shown in Figure 23. Thus, c-Src activation indirectly affects cytoskeletal tension by cross-interacting with RhoA pathway in regulating myosin activity, and has only a modest effect on actin stress fiber morphology. The results of this study suggest that cytoskeletal tension modulation by RhoA and c-Src plays a central role in reinforcing cell adhesion to the matrix. Also, the pre-existing cytoskeletal tension, induced by RhoA activation, directly affects the actomyosin apparatus that modulates the ability of VSMC to adapt to the applied force.

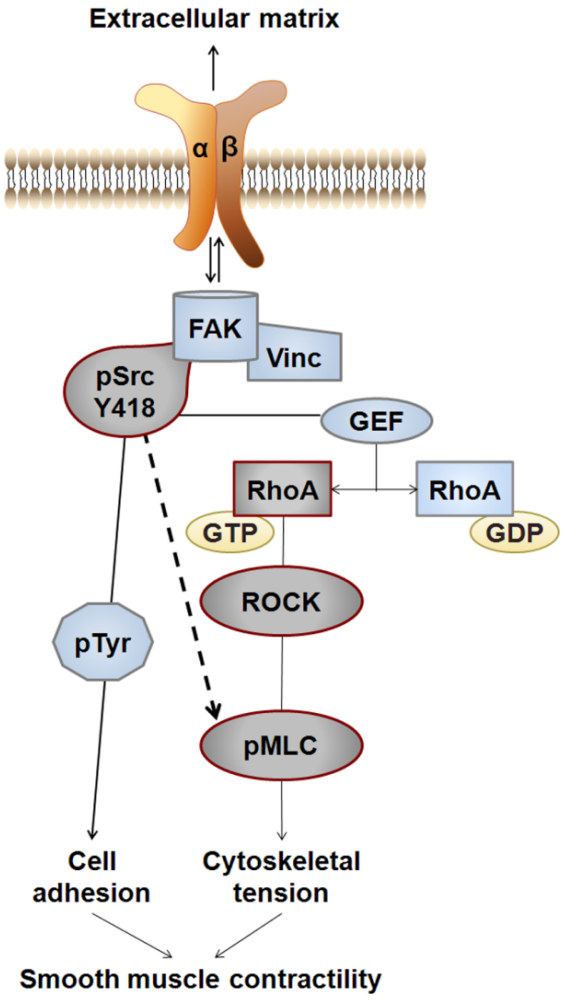

Figure 23: RhoA and Src contribute to cytoskeletal tension regulation.
A subset of focal adhesion proteins that make the link between the extracellular matrix and actin network, with integrins as mechanotransducers, are shown. In addition to the established pathway (thin lines) presenting a direct modulation of cytoskeletal tension by RhoA and cell adhesion by c-Src, the current study presents c-Src as a possible contributor (dashed line) to cytoskeletal tension modulation through regulation of MLC activation downstream of RhoA. Changes in cytoskeletal tension further modulate cell adhesion and smooth muscle contractility. ROCK – Rho kinase; GEF – guanine nucleotide exchange factor; GTP – guanosine triphosphate; GDP – guanosine diphosphate; pTyr – phosphotyrosine; FAK – focal adhesion kinase; Vinc – vinculin. (Reproduced with permission of The Royal Society of Chemistry (RSC) from Sreenivasappa et al., 2014, doi: 10.1039/c4ib00019f)

4.2 Role of Cytoskeletal Tension in Pathogenesis of Occlusive Vascular Diseases

Defects in the normal mechanotransduction process induced by genetic mutation or misregulation of specific proteins disturb the intracellular mechanics and mechanosensory VSMC function, contributing to the initiation or rapid progression of the disease state (Barry et al., 2008).

Actin is a key regulator of VSMC contractility. Actin has six different isoforms of which α-, γ- and β-actin are found in smooth muscle cells. Smooth muscle cell specific α- actin isoform is encoded by ACTA2 gene. Heterozygous mutations in ACTA2 are known to induce hyperplasia of SMC in the neointimal or medial layers of the artery, resulting in occlusive vascular diseases like thoracic aortic aneurysms, including early onset coronary artery disease and stroke, and primary pulmonary hypertension (Guo et al., 2007; Guo et al., 2009; Milewicz et al., 2010).

Pathology of the occlusive arterial lesions in patients with ACTA2 mutations showed increased numbers of VSMC in the neointimal or medial layers of the artery. However, these occlusive lesions lack the lipid and calcium depositions typically found in atherosclerotic lesions (Guo et al., 2009; Stary et al., 1995). Primary cultures of aortic VSMC explanted from patients with ACTA2 mutations showed fewer α-actin fibers when compared with control cells. Additionally, the ACTA2 mutant VSMC in culture proliferate more rapidly when compared with cells explanted from donor controls (Guo et al., 2009). It is known that VSMC proliferation occurs during formation of

atherosclerotic occlusive lesions (Ross and Glomset, 1973; Schwartz et al., 2000), but a role for genetically triggered VSMC hyperplasia as a cause of vascular occlusive disease has been not thoroughly investigated. In order to determine whether the loss of α-smooth muscle actin leads to hyperplasia and determine the molecular pathways responsible for cell proliferation, we sought to investigate the focal adhesion dependent signaling pathway.

4.2.1 Loss of α-actin leads to increased VSMC proliferation and migration

We used α-smooth muscle actin null mouse aortic smooth muscle cells ($Acta2^{-/-}$) as the model system for our study. These $Acta2^{-/-}$ mice were reported to have normal vascular development but compromised vascular contractile force, tone, and blood flow (Schildmeyer et al., 2000). *In vivo* vascular injuries study, using the flow-cessation injury model by which the carotid artery was ligated and tissue was harvested 3 weeks later (Kumar and Lindner, 1997) showed exaggerated neointimal formation in $Acta2^{-/-}$ mice compared to control (Figure 24A). In addition, VSMC isolated from ascending aortas of 4-week-old $Acta2^{-/-}$ mice were compared to wild- type (wt) VSMC *in vitro* (Majesky, 2007). $Acta2^{-/-}$ cells proliferated and migrated more rapidly compared to wt (Figure 24B). Thus, both the *in vivo* and *in vitro* studies performed by Papke et al. (Papke et al., 2013) showed that the loss of α-actin leads to VSMC hyperplasia resulting in increased proliferation. Furthermore, western blot analysis of the cells showed an increase in expression of contractile protein SM22α and calponin-1 in $Acta2^{-/-}$ cells compared to wt (data not shown, Papke et al., 2013).

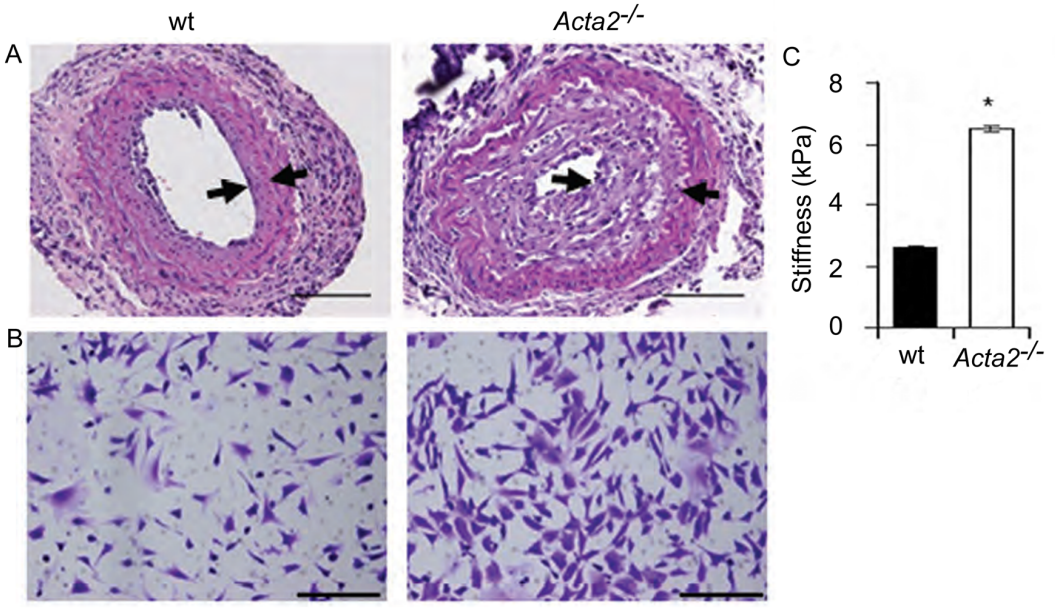

Figure 24: Loss of α-actin leads to increased proliferation, migration, and cytoskeletal tension.
(A) Left carotid arteries were ligated and tissue was harvested 3 weeks post injury. Carotid arteries from Acta2$^{-/-}$ mice (n=7) showed increased neointimal area, ratio of intimal/medial area and degree of stenosis of the lumen compared with carotid arteries obtained from a similar location in wt mice (n = 7). $p < 0.05$. Arrows denote neointimal layer. Scale bars represent 200 μm. (B) Migration assays were performed using 5 ng/ml PDGF-B as a chemoattractant, and showed increased Acta2$^{-/-}$ cells migration compared with wt cells. Five high-powered fields per sample were counted, and data shown are representative of three independent experiments, *$p < 0.05$. Scale bars represent 200 μm. (C) Atomic force microscopy measurements showed that cell stiffness is significantly increased in Acta2$^{-/-}$ VSMC. (*$p<0.05$). Error bars represent ± SD. (Reproduced from Papke CL et al., 2013, Human Molecular Genetics, with permission of Oxford publication, doi:10.1093/hmg/ddt167)

To further understand the effect of α-actin mutation-induced VSMC hyperplasia and increased expression of contractile proteins on the mechanical properties of VSMC, we

used AFM to determine cell stiffness. Interestingly, our studies revealed that Acta2$^{-/-}$ cells measured a 2.5-fold increase in local cell stiffness (i.e., increased cytoskeletal tension) compared to wt (Figure 24C). We suggest that Acta2$^{-/-}$ cells are characterized by an increase in cytoskeletal tension, due to compensatory up-regulation of the other contractile proteins, including an increase in γ-actin expression (unpublished data) which correlates with cell stiffening and proliferation characteristics to occlusive diseases in human patients.

4.2.2 Loss of α-actin is associated with FA remodeling and activation of FA-dependent signaling pathways

Increased cytoskeletal tension is known to drive FA maturation and increased activation of FA-dependent signaling (Goffin et al., 2006). Previous studies have identified increased FAK activity in renal myofibroblasts in Acta2$^{-/-}$ mice (Takeji et al., 2006). In order to understand the effect of α-actin mutation on FA formation and activation, cells were fixed for immunofluorescence by staining with FAK Y397 and vinculin primary antibodies and then were imaged by TIRF microscopy.

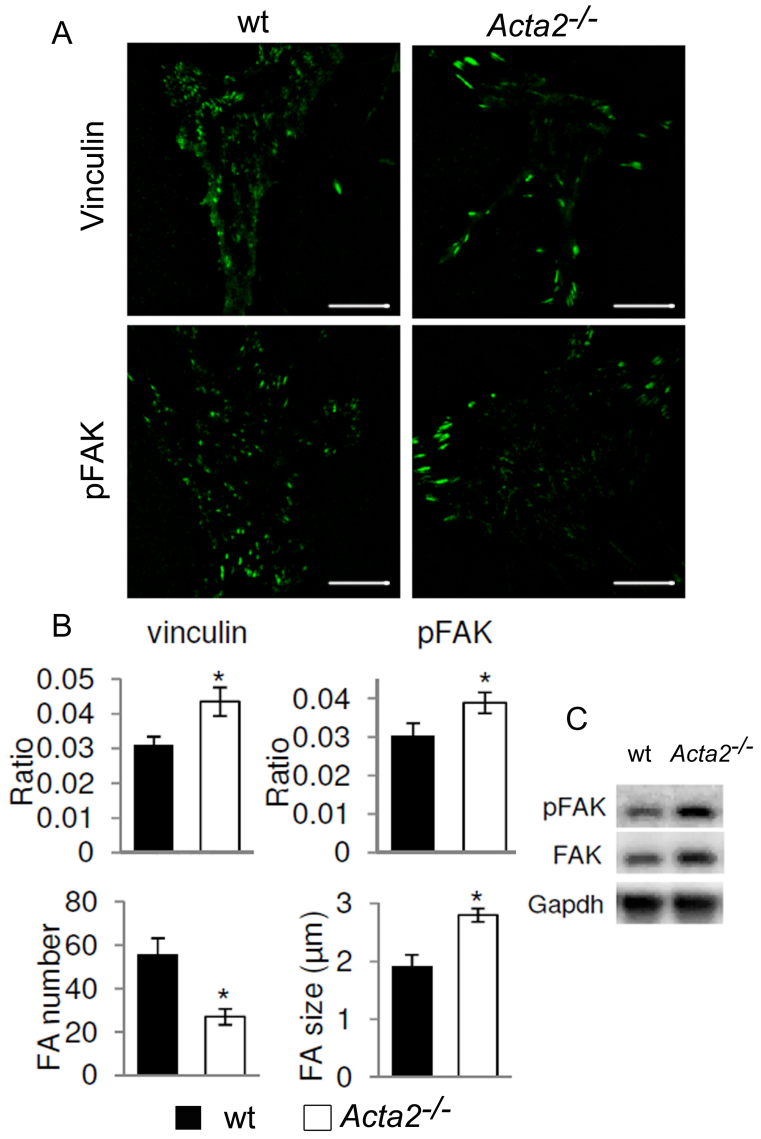

Figure 25: Loss of α-actin leads to alterations in FA formation and activation. (A) Representative TIRF images showing vinculin and pTyr397 FAK. FA were localized to the cell periphery in Acta2$^{-/-}$ cells, whereas they were diffusely located across the cell in the wt cells. Scale bars represent 20 μm. (B) Quantification of vinculin and pFAK relative protein area and individual FA size showed an increase in Acta2$^{-/-}$ cells, but a decrease in the overall number of FA per cell (*$p < 0.05$). (C) Western blots revealed an increase in both FAK and pFAK levels in Acta2$^{-/-}$ cells. (Reproduced from Papke et al., 2013, Human Molecular Genetics, with permission of Oxford publication, doi:10.1093/hmg/ddt167)

Focal adhesions in Acta2$^{-/-}$ cells were observed to accumulate at the cell periphery in contrast to being dispersed across the cell body as in wt. Also, an increase in individual FA size and a decrease in FA number was observed in Acta2$^{-/-}$ cells compared to wt (Figure 25A and B). In addition, Acta2$^{-/-}$ cells measured an increased phosphorylation of FAK Y397, indicating increased FAK activation (Figure 25A and B). These results were independently verified by western blot analysis and were in good agreement with imaging data, showing an increased cellular level of pFAK, along with a corresponding increase in total FAK (Figure 25C). Furthermore, the FA activation measured by TIRF and WB in Acta2$^{-/-}$ cells corresponded well with the increase in stiffness measured by AFM (see Figure 24C)

4.2.3 Discussion

Patients presenting ACTA2 mutations developed occlusive vascular lesions that were characterized by increased numbers of medial or intimal VSMC, but with minimal lipid and calcium deposits, suggesting that VSMC hyperplasia may represent an alternative molecular pathway from a single gene mutation (Guo et al., 2009; Stary et al., 1995). In addition, VSMC explanted from these patients showed a decrease in α-actin and increased proliferation *in vitro* (Guo et al., 2009). In an *in vivo* mouse model (Papke et al., 2013), the loss of α-actin led to excessive neointimal formation with vascular injury, while explanted cells *in vitro* showed an increased proliferation. Additionally, the absence of α-actin in Acta2$^{-/-}$ cells induced an increase in expression of other contractile proteins. Furthermore, α-actin expression and functional stress fiber formation are

required for assembly and maturation of FA in cells, a process driven by FAK (Burridge and Chrzanowska-Wodnicka, 1996; Choi et al., 2008; Geiger and Bershadsky, 2001). However, our FAK and vinculin quantification showed an increase in FA size and number in Acta2$^{-/-}$ cells compared to wt.

RhoA activation is associated with an increase in actin fiber formation, myosin light chain phosphorylation, hence increased cytoskeletal tension. However, in our study no change in activation of RhoA was recorded (data not shown) between Acta2$^{-/-}$ and wt cells (Papke et al., 2013). AFM measurements showed an increase in intracellular tension with loss of α-actin. In visceral organs (e.g., intestine), γ- actin is the major actin isoform expressed by the VSMC, while α-actin is the major isoform expressed in vasculature (Shynlova et al., 2005; Vandekerckhove and Weber, 1978). It has been shown that these two actin isoforms present an opposite up-regulation pattern depending on the VSMC differentiation state (Owens, 1995; Saga et al., 1999). Moreover, the interplay between α- and γ- actin isoforms is directly involved in regulating vascular contractility (Kim et al., 2008). In addition, myosin is involved in cytoskeleton force generation via its central role in cellular contractile properties. VSMC contractility state is mainly determined by the myosin light chain (MLC) phosphorylation level by enabling its molecular interaction with actin (Kaunas and Deguchi, 2011; Sugita et al., 2011). Increased MLC phosphorylation induces contraction of actin fibers due to increased crossbridge activity, while myosin blocking results in reduced crossbridge kinetics (Murphy, 1994). Taken together, these results suggest that the absence of α-

actin may induce compensatory effects of up-regulation of other contractile proteins like calponin and SM22α. In addition, increased expression of Actg2 (unpublished data), suggests that γ-actin is one of the actin isoforms that may compensate the loss of α-actin, which together with increased expression of other contractile proteins, could be responsible for the increased cell stiffness. These results support our hypothesis that FA-dependent signaling pathway and cytoskeleton tension contribute to genetically triggered hyperplastic response of the VSMC resulting in increased risk of occlusive vascular diseases in patients with ACTA2 mutations.

4.3 Role of Nck On Cytoskeletal Tension and Adhesion Strength During Directional Cell Migration

Cellular migration is a complex process that requires a regulated coordination between the actin cytoskeleton and focal adhesions protein activation (Friedl and Wolf, 2010; Gardel et al., 2010; Petrie et al., 2009). Nck (non-catalytic region of tyrosine kinase) adapter proteins are recognized as an important link between tyrosine phosphorylation and actin dynamics (Buday et al., 2002; Lettau et al., 2009); however, the underlying molecular mechanisms and the role of Nck in cytoskeletal remodeling during directional migration remain largely undetermined.

In an effort to understand the role of Nck signaling in cell migration, we used a combination of molecular genetics and quantitative live cell microscopy. Thus, we

studied the effect of Nck on structural, mechanical, and functional properties of the cell cytoskeleton using AFM and fluorescence imaging (Chaki et al. 2013).

4.3.1 Integrin $\alpha_5\beta_1$-fibronectin adhesion force and cell stiffness are modulated by Nck

Nck signaling affects the FA turnover due to formation of unstable multidirectional protrusion in cells (Chaki et al., 2013). To understand this deficiency in coordination of cytoskeletal dynamics during directional migration, we investigated the effect of Nck on structural and mechanical properties of the cell. Adhesion force spectroscopy measurements using an AFM were performed in order to determine the cells stiffness and $\alpha_5\beta_1$-fibronectin adhesion on NIH 3T3 mouse embryonic fibroblasts cells. Cells were transduced with shRNA targeting Nck1 and Nck2 for protein knockdown (i.e. Nck knockdown cells) and rescued by transduction with shRNA-resistant Nck2 (i.e. rescue cells).

As shown in Figure 26A, our adhesion force spectroscopy measurements showed that Nck-deficient cells (deletion of Nck1 and Nck2) were softer (lower cell stiffness) compared to the control and rescue cells. Furthermore, integrin-dependent adhesion force and adhesion probability were significantly decreased in Nck-depleted cells compared to control and rescue cells. These results were consistent with actin protein area measurements performed on fluorescence imaging data which showed well organized actin fibers present in control and rescue cells but not in Nck-depleted cells (Figure 26B). In addition, western blot analysis of Nck-knockdown cells showed a

significant decrease in myosin phosphorylation Ser 19 (Figure 26C) compared to that of control and rescue cells. Taken together, these results suggest that Nck induced stress fibers remodeling modulates cell adhesion and cytoskeletal tension through a mechanism that involves the RhoA pathway.

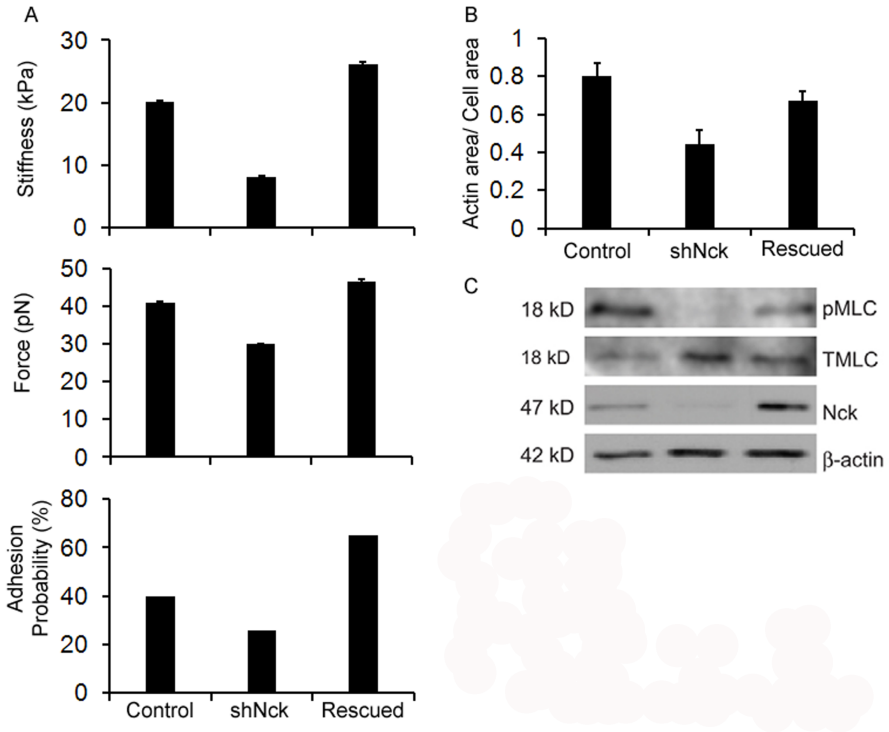

Figure 26: Nck modulates cell adhesion strength to the matrix and cytoskeletal tension. (A) Adhesion force spectroscopy was used to measure local cell stiffness, $\alpha_5\beta_1$ integrin adhesion to fibronectin, and adhesion probability in control, Nck-depleted (shNck1 and 2) and rescued cells. ($p<0.05$). (B) Relative actin ratios from fluorescence images for control, Nck-depleted, and rescued cells (n=6). (C) Representative western blots (top panel) showing myosin II phosphorylation Ser19 (pMLC), total myosin (TMLC), Nck and β-actin. (Reproduced with permission from Journal of Cell Science, Chaki et al., 2013, doi: 10.1242/jcs.119610)

4.3.2 Discussion

Nck represents an important link between tyrosine phosphorylation and actin dynamics, being recognized as a critical mediator of directional migration. The quantitative imaging and molecular studies showed that Nck-depleted cells had critical deficiencies in the coordination of cytoskeletal mechanics due to formation of unstable, multidirectional protrusions, and altered cell–matrix adhesion turnover including impaired maturation of protrusion-associated adhesions. Our results showed that Nck-deficient cells presented a significantly reduced integrin $\alpha_5\beta_1$-fibronectin adhesion force, decreased formation of actin stress fibers, reduced myosin phosphorylation, and decreased cell stiffness (Chaki et al., 2013).

We have shown that RhoA-induced cytoskeletal tension correlates positively with stress fiber formation, integrin activation, and myosin phosphorylation (Lim et al., 2012). Downregulation of Nck signaling leads to a substantive decrease in myosin phosphorylation, which constitutes a novel mechanistic insight provided by this study. In addition, a decrease in RhoA GTPases activation induced by downregulation of Nck signaling was shown through FRET experiments in cells expressing RhoA-Raichu FRET constructs (data not shown, Chaki et al., 2013) This reduction in RhoA activation is consistent with decreased phosphorylation of myosin and actin fiber formation, hence reduced cell stiffness. Moreover, decreased adhesion strength and adhesion probability (i.e. less active integrins) showed lack of maturation of cell-matrix adhesions formed in association with transient protrusions. Taken together, these results suggest that Nck

induces cytoskeletal dysfunction by a mechanism that involves the RhoA pathway, which in turn regulates cell contractility and adhesion.

5 METHODS*

5.1 Vascular Smooth Muscle Cells Culture and Drug Treatments

Vascular smooth muscle cells (VSMC) were isolated from rat cremaster arterioles by Dr. Michael Davis' laboratory, Department of Medical Pharmacology and Physiology, University of Missouri, Columbia, MO as previously described (Wu et al., 2001). Low passage VSMC were cultured in 5% CO_2 at 37 °C in Dulbecco's Modified Eagle Medium (DMEM) supplemented with 10% fetal bovine serum (FBS) and 10 mM HEPES (*Sigma*, St. Louis, MO), 2 mM L-glutamine, 1 mM sodium pyruvate, 100 U/ml penicillin, 100 μg/ml streptomycin, and 0.25 μg/ml amphotericin B. All reagents were purchased from (*Invitrogen,* Carlsbad, CA), unless otherwise specified.

Vascular smooth muscle cells were explanted from mouse aorta of $Acta2^{-/-}$ (α-smooth muscle null) and wt animals in Dr. Dianna M. Milewicz's laboratory, Department of Internal Medicine, University of Texas Health Science Center, Houston, TX as previously described (Cao et al., 2010; Papke et al., 2013). Cells were subcultured in Smooth Muscle Basal Media (*Lonza*, Koeln, Germany) containing 20% FBS (*Atlanta Biologicals,* Flowery Branch, GA), pyruvate, HEPES, L-glutamine, antibiotic and growth factors (SmBM Bullet Kit; *Lonza*).

* Text reproduced with permission of The Royal Society of Chemistry (RSC) from Sreenivasappa et al., 2014, doi: 10.1039/c4ib00019f. Part of text reproduced with permission of The Royal Society of Chemistry (RSC) from Lim et al., 2012, doi: 10.1039/c2ib20008b

For drug treatment, cells were supplemented with 1% FBS cell culture medium 5 hours after initial plating of the cells. Before imaging, the serum-depleted medium was supplemented with respective drugs for corresponding incubation time for each experiment as listed in Table 1.

Table 1 Drug Treatment Conditions.

Drug	Concentration	Incubation	Company
LPA	10 μM (*FL*) 15 μM (*WB*)	1h at RT 45 min at RT	Sigma-Aldrich
Y-27632	10 μM (*FL*) 40 μM (*WB*)	1h at RT 45 min at RT	Sigma-Aldrich
ML-7	1 μM (*AFM*) or 20 μM (*FL*) 10 μM (*WB*)	10 min at 37 °C, 1h at RT Overnight at 37 °C	Sigma-Aldrich
SU6656	5 μM (*AFM*) 5 μM (*FL/WB*)	1.5 h at 37 °C, 30min at RT 2 h at 37 °C	Millipore

FL – Fluorescence imaging, AFM – adhesion force spectroscopy, WB – Western blot

5.2 Live Cell Fluorescence Imaging

5.2.1 Transient transfections

Transient transfections of cells in suspension were performed using the Nucleofector apparatus (*Lonza*, Koeln, Germany) with Nucleofector kit VPI-1004. As recommended in the manufacturers' protocol, 500K cells per reaction were transfected with GFP plasmids and subsequently plated on 60 or 35 mm *MatTek* dishes (*Ashland*, MA, USA)

and incubated overnight in 5% CO_2 at 37 °C (Lim et al., 2010). All imaging experiments were performed in phenol-red free DMEM (*Invitrogen,* Carlsbad, CA), at room temperature.

5.2.2 Fluorescence reporter constructs

RhoA plasmid constructs pcDNA3-EGFP-RhoA-wt (wild type), pcDNA3-EGFP-RhoA-T19N (dominant negative), and pcDNA3-EGFP-RhoA-Q63L (constitutively active) (Subauste et al., 2000) used for this work were purchased from Addgene plasmid repository (Cambridge, MA, USA). Actin-mRFP plasmid was a gift of Michael Davidson (*Florida State University*, Tallahassee, FL); vinculin-GFP plasmid was a gift of Kenneth Yamada (*National Institutes of Health, National Institute of Dental and Craniofacial Research*, Bethesda, MD); Src Homology 2 domains fused to EYFP (dSH2-EYFP) (Kirchner et al., 2003) was a gift of Benjamin Geiger (*Weizmann Institute of Science*, Rehovot, Israel); and c-Src-wt-EGFP (wild-type chicken c-Src) plasmid was a gift from Marylin Resh (*Memorial Sloan-Kettering Cancer Center*, New York, NY).

Our collaborator, Dr. Gonzalo M. Rivera, Department of Veterinary Pathobiology, Texas A&M University, College Station, TX designed and made corresponding mCherry constructs for c-Src-EGFP and dSH2-EGFP constructs and Src-Y530F CA mutations (Sreenivasappa et al., 2014). Our collaborator, Dr. Michael W. Davidson, of National High Magnetic Field Laboratory, Florida State University, Tallahassee, Florida designed and made c-Src dominant negative EGFP construct (Sreenivasappa et al., 2014).

5.3 Immunofluorescence

VSMC were cultured in the same conditions as above and after 24 h cells were fixed by immersion in 2% paraformaldehyde in DPBS followed by washing in a glycine buffer. Cells were incubated overnight at 4 °C with an appropriate primary antibody directed to the protein of interest. After washing, cells were incubated with a fluorophore-labeled secondary antibody for 1 h at room temperature, followed by another washing. All antibodies were diluted in a sodium citrate buffer containing BSA (Sun et al., 2005). Labeled cells were immersed in DPBS and imaged immediately. Primary and secondary antibodies that were used are listed in Table 2.

Table 2 Immunofluorescence Antibodies

Primary antibodies	
Name	**Company**
anti-FAK-Y397	611806, BD Bioscience
anti-pTyr	F3145, Sigma-Aldrich
anti-actin	A5228, Sigma-Aldrich
anti-vinculin	V9131Sigma-Aldrich
Secondary antibodies	
Alexa 488	A11008, Invitrogen
Alexa 568	A11011, Invitrogen

5.4 Fluorescence Image Analysis

Quantitative measurements of protein area from fluorescence images were performed by measuring the fluorescence intensity. TIRF images were used to determine the protein area at the basal cell surface (dSH2, vinculin, pTyr, pFAK, etc.) and projections of confocal images were used to measure actin area throughout the cell. Protein area and FA parameters were measured by using the masking tool and image statistics tools in the SlideBook software (*Intelligent Imaging Innovations*, Denver, CO). The fluorescence measurements correlated directly with the amount of protein present at FA or actin filaments, representing a measure of the relative protein density at the specific sites (Ballestrem et al., 2001). In order to compare a large number of cells, the fluorescence protein area was normalized to the total cell area for each cell before statistical analysis.

5.5 Adhesion Force Spectroscopy Using Atomic Force Microscope

5.5.1 Probe functionalization

Unsharpened silicon nitride cantilevers (MLCT-AUHW) from *Bruker Nano Surfaces* (formerly *Veeco Instruments*, Santa Barbara, CA, USA) with a spring constant of 12.2 ± 0.4 pN/nm were used. The cantilever spring constant was calibrated in liquid using the thermal noise analysis (Butt and Jaschke, 1995; Hutter and Bechhoefer J, 1993) available on the XZ Hybrid Bioscope AFM system (*Bruker Nano Surfaces*, Santa Barbara, CA). For adhesion force spectroscopy the pyramidal tip was coated with 1 mg/ml fibronectin (FN, 33016-015, *Invitrogen,* Carlsbad, CA) using 10 mg/ml polyethylene glycol (PEG, P4463, *Sigma*, St. Louis, MO) as a cross-linker (Trache and Meininger, 2008a). The

probe was mounted onto the glass holder and washed five times with deionized water. Next, the probe was incubated with PEG for 5 min and then washed again five times with deionized water. Following the wash, the tip was incubated with FN for 3 min, and then washed again five times with Dulbecco's Phosphate buffered saline (DPBS). The functionalized probe was then mounted on the AFM scanning head. The spring constant of the cantilever was assumed to be unchanged after the protein labeling.

5.5.2 Adhesion force spectroscopy measurements and data analysis

For adhesion force spectroscopy measurements the AFM was operated in force mode. The AFM probes functionalized with fibronectin were driven to touch and retract from the cell surface over a known predefined distance in the z-axis with a frequency of 0.5 Hz. The z-axis movement and the deflection of the cantilever were recorded in a force curve. The measurements were performed in a region midway between the nucleus and the edge of the cell. Data were acquired for 2 min per cell and repeated for 10 cells per dish, for 4-6 different dishes per condition, generating ~ 2,000-4,000 individual measurements for each case. The adhesion force was calculated by multiplying the change in deflection height associated with the unbinding event by the spring constant of the cantilever. In previous AFM studies on VSMC we have shown that FN-$\alpha_5\beta_1$ integrin interaction is specific (Sun et al., 2005) The local cell stiffness at the point of contact was calculated as Young's modulus of elasticity, by fitting the approach curve between the initial point of cell contact and point of maximum probe displacement with Sneddon's modified Hertz model (Trache et al. 2005, see Section 3.1.2.2.2)

5.6 Mechanical Stimulation Using Atomic Force Microscope

5.6.1 Probe functionalization

For mechanical stimulation of live cells, a 2-micron glass bead functionalized with biotin was attached to a flat silicon nitride cantilever (*Novascan Technologies*, IA, USA). The bead was functionalized with laminin (LN) or fibronectin (FN). The bead was first coated with 1 mg/ml avidin (*Sigma*, St. Louis, USA) and then cross-linked with biotinylated ECM protein. The coating was performed only at the very end of the cantilever to avoid altering its spring constant that is assumed to be unchanged after protein labeling (10.2 ± 2.2 pN/nm). The biotinylated ECM was prepared by mixing 1 mg/ml FN (F4759, *Sigma*, St. Louis, USA) or LN (L2020, *Sigma*, St. Louis, USA) with 10 mg/ml Sulfo-NHS-LC-Biotin (21335, *Pierce*, Rockford, IL, USA), and then kept on ice for 2 h. Unbound biotin was separated by centrifugation with a Microcon YM-30 filter set (42422, *Millipore*, Billerica, MA, USA).

5.6.2 Tensile stress mechanical stimulation and data analysis

For tensile stress stimulation of VSMC the AFM was used in contact imaging mode. The ECM functionalized AFM probe was placed at an x-y coordinate on the cell surface and kept in place for 20 min to allow the ECM to initiate formation of a FA. The mechanical stimulation consisted of controlled upward movement of the cantilever in discrete steps at 3–5 min intervals over 80 min. The force magnitude applied by the AFM can be varied between 0.1–10 nN. After the initial priming period with low level forces (<0.4 nN), ~0.5 nN and ~1 nN forces were applied in a series of discrete steps. The cell

response was recorded in a series of 512 X 512 pixel images, each line in the image representing a unit time of 1 s (Lim et al., 2012; Trache and Lim, 2010). Bead displacement data correspond to the true height change of the piezo needed to maintain constant cantilever deflection. This condition is attained by using high values for the feedback gains, such that the piezo height will change to keep the photodiode output close to the setpoint, therefore the cantilever deflection remains nearly constant. The setpoint can be adjusted to increase or decrease the cantilever deflection and, therefore, the applied force of the probe on the sample. The data were acquired in Nanoscope software and were processed off-line in MatLab (*Mathworks, Inc.*) or Autosignal (*Systat Software Inc.*, San Jose, CA) and Excel (*Microsoft*, Redmond, WA).

5.7 Statistical Data Analysis

5.7.1 Fluorescence intensity measurements

Student's t-test and/or multi-way analysis of variance (ANOVA) were used for statistical analysis. Log-transforms were applied as necessary to the response variables to ensure normality of the distributions prior to running the ANOVA. Pre-planned comparisons among means were performed via single degree of freedom contrasts using the ANOVA model coefficients. All statistical differences were considered significant at $p < 0.05$.

5.7.2 Adhesion force spectroscopy

Kernel density plots of the distribution of adhesion force and elasticity measurements were generated in NForceR software (Trzeciakowski and Meininger, 2004). Normal

reference bandwidths and Gaussian kernel functions (Silverman, 1986) were used. These data were further analyzed using PeakFit (v4.11, *Systat Software Inc.,* Chicago, IL) to provide accurate estimates of the peak value and associated confidence intervals for each distribution. The peaks whose confidence intervals did not overlap were considered significantly different ($p < 0.05$) (Venables and Ripley, 1994)

5.8 Western Blotting

Cells were plated on 60 mm cell culture dishes as described above and allowed to attach to the substrate for 24 h. For drug treatment, the concentrations and incubation time were followed as described in Table 1. For total protein lysate, cells were lysed with RIPA lysis buffer (Lim et al., 2010). To separate cytoskeletal and cytoplasmic fractions, Triton X-100 lysis buffer (Lim et al., 2010) was added to the cell. The supernatant was then removed and designated the cytoplasmic fraction. To retrieve the cytoskeletal fraction, RIPA lysis buffer was added and the dish was scraped vigorously. In order to compare phosphorylated proteins in cell cytoplasm and cytoskeleton, the same fractionation protocol was followed with the exception that the lysis buffers were supplemented with a protease inhibitor cocktail (Lim et al., 2010). Immunoblotting was performed with specific antibodies as listed in Table 3. All lysates were analyzed by SDS-PAGE using a NuPAGE Bis–Tris gel (*Invitrogen*, Carlsbad, CA) and the proteins were electrophoretically transferred to nitrocellulose membrane. Triplicate experiments were conducted on different days, and blots were analyzed by quantitative densitometry using ImageJ software (Rasband, 1997-2004).

Table 3 Western Blot Antibodies

Primary antibodies	
Name	**Company**
anti-actin	A5228, Sigma-Aldrich
anti-vinculin	V9131Sigma-Aldrich
anti- MLC- Ser19 (pMLC)	3675S, Cell Signaling Tech. Inc.
anti-MLC (MLC/TMLC)	3672, Cell Signaling Tech. Inc.
anti-GAPDH	MAB374, Millipore;Fitzgerald; 437000, Invitrogen
anti-Src Y418	S1940, Sigma-Aldrich
anti-p397FAK	04-974, Millipore
anti-FAK	Santa Cruz Biotechnology
anti-Nck	610099, BD Biosciences
anti β- actin	A1978, Sigma
Secondary antibodies	
donkey anti- rabbit mouse horseradish peroxidase	711-035-152, Jackson Immuno Research
goat anti-mouse horseradish peroxidase	1858413, Pierce Antibodies sc-2055, Santa Cruz Biotechnology

5.9 Histology

Aortas were isolated from mice and cleaned from adventitia and blood and immersed in 10% formalin overnight, then transferred to 70% ethanol and kept at 4 ºC until futher processing. The specimen was further processed by dehydrating and embedding in a

paraffin block. The embedded specimen was further sectioned at 5 μm, deparaffinized, rehydrated, and stained for histology. Separate slides were stained with Verhoef van Gieson (VVG) for elastin, hematoxylin and eosin (H&E) counter staining for tissue morphology, and Masson's Trichrome (TRI) for collagen. Images were captured with Olympus CH2 microscope equipped with a color camera (Motic) and a 20x objective.

6 CONCLUSIONS

Our study focused on understanding in real-time how cells sense and adapt to extracellular mechanical cues in the context of cellular dynamic remodeling. In order to accomplish our objective, we analyzed the relationship between cytoskeletal tension and cell-matrix adhesion using a combination of single ligand–receptor interaction measurements and fluorescence imaging on live VSMC.

In Section 4.1 we investigated the relationship between the cytoskeletal tension and integrin $\alpha_5\beta_1$ adhesion strength to the matrix (i.e., fibronectin) in the context of RhoA–Src crosstalk (Figure 27A). Single ligand–receptor interaction measurements performed with AFM probes functionalized with fibronectin showed that RhoA and c-Src activation have different effects on cytoskeletal tension development, inducing two distinct force–stiffness functional regimes for $\alpha_5\beta_1$-integrin binding to fibronectin. Moreover, fluorescence measurements showed that c-Src activation had a modest effect on actin morphology, while RhoA significantly modulated stress fiber formation. In addition, c-Src was associated with regulation of myosin light chain (MLC) phosphorylation, suggesting a c-Src-dependent modulation of RhoA pathway through activation of downstream effectors. Therefore, c-Src may be a possible component of cytoskeletal tension regulation through myosin activation. Our findings suggest that Src and RhoA coordinate a regulatory network that determines cytoskeletal tension through activation

of actomyosin contractility. In turn, the cytoskeletal tension state modulates integrin $\alpha_5\beta_1$–fibronectin adhesion force.

The work presented in Section 4.2 suggests a novel signaling pathway that links loss of α-actin with compensatory mechanisms for supplementing the reduced actomyosin contractility through up-regulation of other contractile proteins, and increased FAK activation, resulting in increased proliferation and migration (Figure 27B). Our findings in Section 4.3 suggest that Nck regulates directional cell migration in part through modulation of cytoskeletal tension and cell-matrix adhesion strength, which has an important role in coordination of cytoskeletal mechanics through a mechanism that also involves the RhoA pathway (Figure 27C).

In conclusion, our studies highlight a central role for cytoskeletal tension in modulating cytoskeletal dynamics and cell adhesion to the matrix.

6.1 Future Work

Our studies have narrowed the knowledge gap and opened a new path to understanding at the sub-cellular level VSMC cytoskeletal tension development in the context of cellular contractility and cell proliferation in order to explain vascular wall remodeling in disease progression. Our findings also highlight the importance of further investigations of RhoA pathway crosstalk in cellular signaling network. We suggest a follow up of this work with a set of experiments involving AFM mechanical stimulation

and stretch experiments to dissect further cytoskeletal tension development as a result of cellular adaptation to their microenvironment. The recent developments in Forster resonance energy transfer (FRET) sensors present a great resource to understand spatio-temporal activation of the mechanical signaling pathway in response to mechanical stimulation. Furthermore, studies will be directed toward understanding the cell's ability to sense and adapt to changes in the extracellular matrix stiffness characteristic to disease states by studying key cytoskeletal proteins and adhesion molecules.

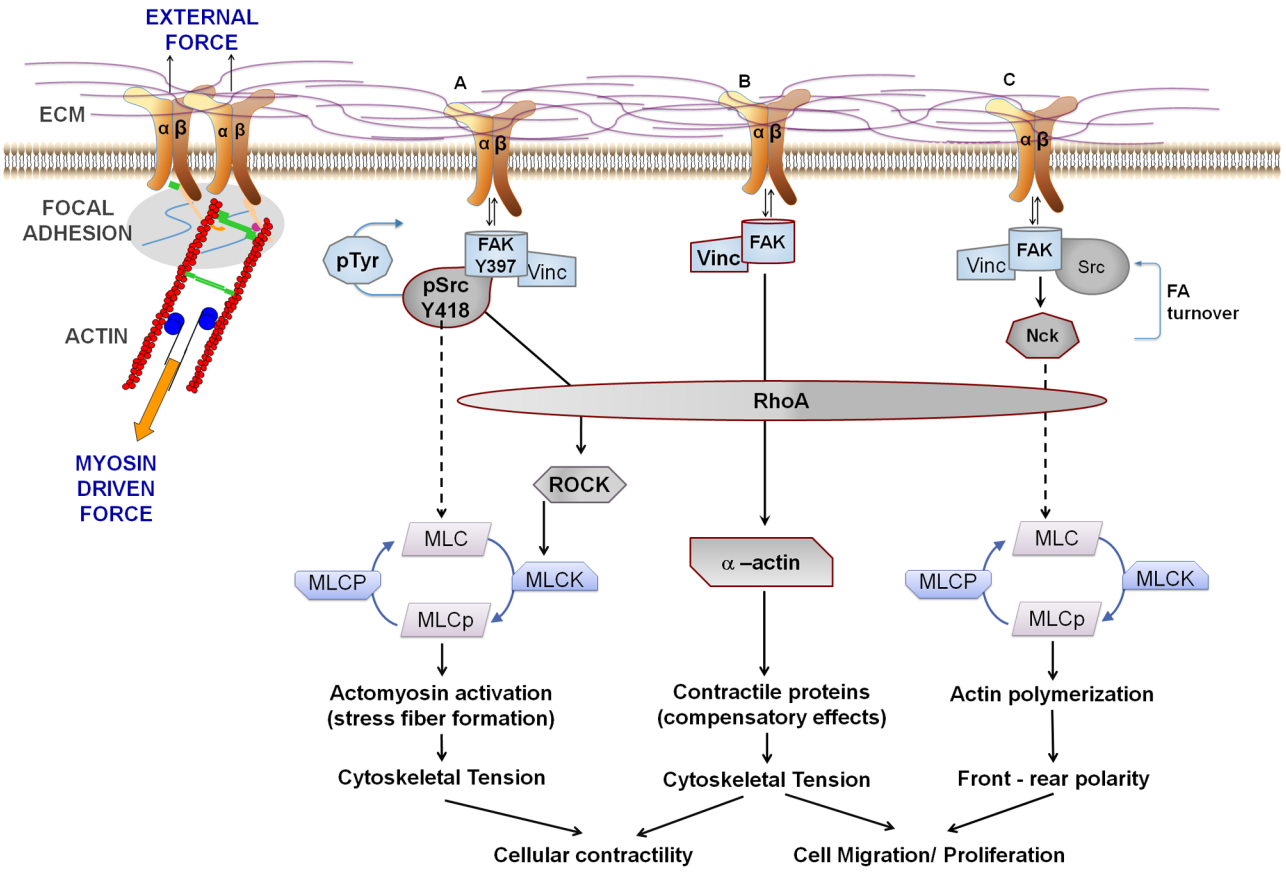

Figure 27: Summary schematic.
RhoA is a key element in determining contractility state of the cell. Cytoskeletal tension has a central role in modulating cytoskeleton dynamics and cell adhesion to the matrix.

REFERENCES

Amano, M., Chihara, K., Kimura, K., Fukata, Y., Nakamura, N., Matsuura, Y. and Kaibuchi, K. (1997). Formation of actin stress fibers and focal adhesions enhanced by rho-kinase. *Science*. **275**, 1308-1311.

Amano, M., Ito, M., Kimura, K., Fukata, Y., Chihara, K., Nakano, T., Matsuura, Y. and Kaibuchi, K. (1996). Phosphorylation and activation of myosin by rho-associated kinase (rho-kinase). *J. Biol. Chem*. **271**, 20246-20249.

Arias-Salgado, E. G., Lizano, S., Sarkar, S., Brugge, J. S., Ginsberg, M. H. and Shattil, S. J. (2003). Src kinase activation by direct interaction with the integrin beta cytoplasmic domain. *Proc. Natl. Acad. Sci. U S A*. **100**, 13298-13302.

Axelrod, D. (2001a). Total internal reflection fluorescence microscopy. In *Methods in Cellular Imaging*. (ed. A. Periasamy), pp. 362-380. New York: Springer.

Axelrod, D. (2001b). Total internal reflection fluorescence microscopy in cell biology. *Traffic*. **2**, 764-774.

Axelrod, D. (2003). Total internal reflection fluorescence microscopy in cell biology. *Methods Enzymol*. **361**, 1-33.

Axelrod, D. (2008). Chapter 7: Total internal reflection fluorescence microscopy. *Methods Cell Biol*. **89**, 169-221.

Axelrod, D., Burghardt, T. P. and Thompson, N. L. (1984). Total internal reflection fluorescence. *Annu Rev. Biophys. Bioeng*. **13**, 247-268.

Axelrod, D., Thompson, N. L. and Burghardt, T. P. (1983). Total internal inflection fluorescent microscopy. *J. Microsc*. **129**, 19-28.

Ballestrem, C., Erez, N., Kirchner, J., Kam, Z., Bershadsky, A. and Geiger, B. (2006). Molecular mapping of tyrosine-phosphorylated proteins in focal adhesions using fluorescence resonance energy transfer. *J. Cell Sci*. **119**, 866-875.

Ballestrem, C., Hinz, B., Imhof, B. A. and Wehrle-Haller, B. (2001). Marching at the front and dragging behind: Differential αvβ3-integrin turnover regulates focal adhesion behavior. *J. Cell Biol*. **155**, 1319-1332.

Barry, S. P., Davidson, S. M. and Townsend, P. A. (2008). Molecular regulation of cardiac hypertrophy. *Intl. J. Biochem. Cell Biol*. **40**, 2023-2039.

Beevers, G., Lip, G.Y. and O'Brien, E. (2001). Abc of hypertension: Blood pressure measurement. Part II-conventional sphygmomanometry: Technique of auscultatory blood pressure measurement. *BMJ*. **322**, 1043-1047.

Bertocchi, C., Goh, W. I., Zhang, Z. and Kanchanawong, P. (2013). Nanoscale imaging by superresolution fluorescence microscopy and its emerging applications in biomedical research. *Crit. Rev. Biomed. Eng.* **41**, 281-308.

Bi, D., Nishimura, J., Niiro, N., Hirano, K. and Kanaide, H. (2005). Contractile properties of the cultured vascular smooth muscle cells: The crucial role played by rhoa in the regulation of contractility. *Circ. Res*. **96**, 890-897.

Binnig, G., Quate, C. F. and Gerber, C. (1986). Atomic force microscope. *Phys. Rev.*

Lett. **56**, 930-933.

Blake, R. A., Broome, M. A., Liu, X., Wu, J., Gishizky, M., Sun, L. and Courtneidge, S. A. (2000). Su6656, a selective src family kinase inhibitor, used to probe growth factor signaling. *Mol. Cell Biol*. **20**, 9018-9027.

Bolz, S. S., Vogel, L., Sollinger, D., Derwand, R., Boer, C., Pitson, S. M., Spiegel, S. and Pohl, U. (2003). Sphingosine kinase modulates microvascular tone and myogenic responses through activation of Rhoa/Rho kinase. *Circulation*. **108**, 342-347.

Borisy, G. G. and Svitkina, T. M. (2000). Actin machinery: Pushing the envelope. *Curr. Opin. Cell Biol*. **12**, 104-112.

Braga, P. C. and Ricci, D. (2004). Atomic force microscopy: Biomedical methods and applications. Totowa, N.J: Humana Press.

Buday, L., Wunderlich, L. and Tamas, P. (2002). The nck family of adapter proteins: Regulators of actin cytoskeleton. *Cell Signal*. **14**, 723-731.

Burridge, K. and Wennerberg, K. (2004). Rho and Rac take center stage. *Cell*. **116**, 167-179.

Burridge, K., and Chrzanowska-Wodnicka, M. (1996). Focal adhesions, contractility, and signaling. *Annu Rev Cell Dev Biol*. **12**:463-518.

Butt, H. J. and Jaschke, M. (1995). Calculation of thermal noise in atomic force microscopy. *Nanotechnology*. **6**, 1-7.

Cao, J., Gong, L., Guo, D. C., Mietzsch, U., Kuang, S. Q., Kwartler, C. S., Safi, H., Estrera, A., Gambello, M. J. and Milewicz, D. M. (2010). Thoracic aortic disease in tuberous sclerosis complex: Molecular pathogenesis and potential therapies in TSC2+/- mice. *Hum. Mol. Genet*. **19**, 1908-1920.

Cerutis, D. R., Nogami, M., Anderson, J. L., Churchill, J. D., Romberger, D. J., Rennard, S. I. and Toews, M. L. (1997). Lysophosphatidic acid and egf stimulate mitogenesis in human airway smooth muscle cells. *Am. J. Physiol*. **273**, L10-15.

Chaki, S. P., Barhoumi, R., Berginski, M. E., Sreenivasappa, H., Trache, A., Gomez, S. M. and Rivera, G. M. (2013). Nck enables directional cell migration through the coordination of polarized membrane protrusion with adhesion dynamics. *J. Cell Sci*. **126**, 1637-1649.

Chen, C. S., Tan, J. and Tien, J. (2004). Mechanotransduction at cell-matrix and cell-cell contacts. *Annu. Rev. Biomed. Eng*. **6**, 275-302.

Chen, C.S. (2008). Mechanotransduction - a field pulling together? *J Cell Sci*. **121**:3285-92.

Chiang, H.-Y., Korshunov, V. A., Serour, A., Shi, F. and Sottile, J. (2009). Fibronectin is an important regulator of flow-induced vascular remodeling. *Arterioscler. Thromb. Vasc. Biol*. **29**, 1074-1079.

Choi, C. K., Vicente-Manzanares, M., Zareno, J., Whitmore, L. A., Mogilner, A. and Horwitz, A. R. (2008). Actin and alpha-actinin orchestrate the assembly and

maturation of nascent adhesions in a myosin II motor-independent manner. *Nat. Cell Biol*. **10**, 1039-1050.

Cines, D. B., Pollak, E. S., Buck, C. A., Loscalzo, J., Zimmerman, G. A., McEver, R. P., Pober, J. S., Wick, T. M., Konkle, B. A., Schwartz, B. S., Barnathan, E. S., McCrae, K. R., Hug, B. A., Schmidt, A. M. and Stern, D. M. (1998). Endothelial cells in physiology and in the pathophysiology of vascular disorders. *Blood*. **91**, 3527-3561.

Danen, E. H., van Rheenen, J., Franken, W., Huveneers, S., Sonneveld, P., Jalink, K. and Sonnenberg, A. (2005). Integrins control motile strategy through a Rho-cofilin pathway. *J. Cell Biol*. **169**, 515-526.

D'Angelo, G., Mogford, J. E., Davis, G. E., Davis, M. J., and Meininger, G. A. (1997). Integrin-mediated reduction in vascular smooth muscle [Ca2+]i induced by RGD-containing peptide. *Am. J. Physiol*. **272**, H2065-H2070.

Davis, M. J., Wu, X., Nurkiewicz, T. R., Kawasaki, J., Davis, G. E., Hill, M. A. and Meininger, G. A. (2001). Integrins and mechanotransduction of the vascular myogenic response. *Am. J. Physiol. Heart Circ. Physiol*. **280**, H1427-H1433.

del Rio, A., Perez-Jimenez, R., Liu, R., Roca-Cusachs, P., Fernandez, J. M. and Sheetz, M. P. (2009). Stretching single talin rod molecules activates vinculin binding. *Science*. **323**, 638-641.

Dubash, A. D., Menold, M. M., Samson, T., Boulter, E., Garcia-Mata, R., Doughman, R. and Burridge, K. (2009). Chapter 1. Focal adhesions: new

angles on an old structure. *Int. Rev. Cell Mol. Biol*. **277**, 1-65.

Engler, A. J., Humbert, P. O., Wehrle-Haller, B. and Weaver, V. M. (2009). Multiscale modeling of form and function. *Science*. **324**, 208-212.

Eriksson, J.E., Dechat, T., Grin, B., Helfand, B., Mendez, M., Pallari, H. M. and Goldman, R. D. (2009). Introducing intermediate filaments: from discovery to disease. *J. Clin. Invest*. **119**, 1763-1771.

Etienne-Manneville, S. (2010). From signaling pathways to microtubule dynamics: the key players. *Curr. Opin. Cell Biol*. **22**, 104-11.

Evans, E. A. and Calderwood, D. A. (2007). Forces and bond dynamics in cell adhesion. *Science*. **316**, 1148-1153.

Farr, G. A., Hull, M., Mellman, I. and Caplan, M. J. (2009). Membrane proteins follow multiple pathways to the basolateral cell surface in polarized epithelial cells. *J. Cell. Biol*. **186**, 269-282.

Felsenfeld, D. P., Schwartzberg, P. L., Venegas, A., Tse, R. and Sheetz, M. P. (1999). Selective regulation of integrin-cytoskeleton interactions by the tyrosine kinase Src. *Nat. Cell Biol*. **1**, 200-206.

Friedl, P. and Wolf, K. (2010). Plasticity of cell migration: a multiscale tuning model. *J. Cell Biol*. **188**, 11-19.

Friedland, J. C., Lee, M. H. and Boettiger, D. (2009). Mechanically activated integrin switch controls alpha5beta1 function. *Science*. **323**, 642-644.

Gardel, M. L., Schneider, I. C., Aratyn-Schaus, Y. and Waterman, C. M. (2010). Mechanical integration of actin and adhesion dynamics in cell migration. *Annu. Rev. Cell Dev. Biol*. **26**, 315-333.

Geiger, B. and Bershadsky, A. (2001). Assembly and mechanosensory function of focal contacts. *Curr. Opin. Cell Biol*. **13**, 584-592.

Gimbrone, M. A., Jr. Anderson, K. R., Topper, J. N., Langille, B. L., Clowes, A. W., Bercel, S., Davies, M. G., Stenmark, K. R., Frid, M. G., Weiser-Evans, M. C., Aldashev, A. A., Nemenoff, R. A., Majesky, M. W., Landerholm, T. E., Lu, J., Ito, W. D., Arras, M., Scholz, D., Imhof, B., Aurrand-Lions, M., Schaper, W., Nagel, T. E., Resnick, N., Dewey, C. F., Gimbrone, M. A. and Davies, P. F. (1999). Special communication the critical role of mechanical forces in blood vessel development, physiology and pathology. *J. Vasc. Surg*. **29**, 1104-1151.

Glukhova, M. A. and Koteliansky, V. E. (1995). Integrins, cytoskeletal and extracellular matrix proteins in developing smooth muscle cells of human aorta. In: *The Vascular Smooth Muscle Cell* (ed S. M. S. P. Mecham), pp. 37-79. San Diego, CA: Academic Press.

Go, A. S., Mozaffarian, D., Roger, V. L., Benjamin, E. J., Berry, J. D., Blaha, M. J., Dai, S., Ford, E. S., Fox, C. S., Franco, S., Fullerton, H. J., Gillespie, C., Hailpern, S. M., Heit, J. A., Howard, V. J., Huffman, M. D., Judd, S. E., Kissela, B. M., Kittner, S. J., Lackland, D. T., Lichtman, J. H., Lisabeth, L.

D., Mackey, R. H., Magid, D. J., Marcus, G. M., Marelli, A., Matchar, D. B., McGuire, D. K., Mohler, E. R., Moy, C. S., Mussolino, M. E., Neumar, R. W., Nichol, G., Pandey, D. K., Paynter, N. P., Reeves, M. J., Sorlie, P. D., Stein, J., Towfighi, A., Turan, T. N., Virani, S. S., Wong, N. D., Woo, D. and Turner, M. B. (2014). Heart disease and stroke statistics—2014 update: a report from the American Heart Association. *Circulation*. **129**, e28-e292.

Goffin, J. M., Pittet, P., Csucs, G., Lussi, J. W., Meister, J. J. and Hinz, B. (2006). Focal adhesion size controls tension-dependent recruitment of alpha-smooth muscle actin to stress fibers. *J. Cell Biol*. **172**, 259-268.

Gokina, N. I., Park, K. M., McElroy-Yaggy, K. and Osol, G. (2005). Effects of rho kinase inhibition on cerebral artery myogenic tone and reactivity. *J. Appl. Physiol.* **98**, 1940-1948.

Goldschmidt, M. E., McLeod, K. J. and Taylor, W. R. (2001). Integrin-mediated mechanotransduction in vascular smooth muscle cells: frequency and force response characteristics. *Circ. Res*. **88**, 674-680.

Graf, R., Rietdorf, J. and Zimmermann, T. (2005). Live cell spinning disk microscopy. *Adv. Biochem. Eng. Biotechnol*. **95**, 57-75.

Gunst, S. J. and Fredberg, J. J. (2003). The first three minutes: smooth muscle contraction, cytoskeletal events and soft glasses. *J. Appl. Physiol. (1985)*. **95**, 413-425.

Gunst, S. J., Tang, D. D. and Opazo Saez, A. (2003). Cytoskeletal remodeling of the

airway smooth muscle cell: a mechanism for adaptation to mechanical forces in the lung. *Respir. Physiol. Neurobiol*. **137**, 151-168.

Gunst, S. J. and Zhang, W. (2008). Actin cytoskeletal dynamics in smooth muscle: a new paradigm for the regulation of smooth muscle contraction. *Am. J. Physiol. Cell Physiol*. **295**, C576-C587.

Guo, D. C., Pannu, H., Tran-Fadulu, V., Papke, C. L., Yu, R. K., Avidan, N., Bourgeois, S., Estrera, A. L., Safi, H. J., Sparks, E., Amor, D., Ades, L., McConnell, V., Willoughby, C. E., Abuelo, D., Willing, M., Lewis, R. A., Kim, D. H., Scherer, S., Tung, P. P., Ahn, C., Buja, L. M., Raman, C. S., Shete, S. S. and Milewicz, D. M. (2007). Mutations in smooth muscle alpha-actin (acta2) lead to thoracic aortic aneurysms and dissections. *Nat. Genet*. **39**, 1488-1493.

Guo, D. C., Papke, C. L., Tran-Fadulu, V., Regalado, E. S., Avidan, N., Johnson, R. J., Kim, D. H., Pannu, H., Willing, M. C., Sparks, E., Pyeritz, R. E., Singh, M. N., Dalman, R. L., Grotta, J. C., Marian, A. J., Boerwinkle, E. A., Frazier, L. Q., LeMaire, S. A., Coselli, J. S., Estrera, A. L., Safi, H. J., Veeraraghavan, S., Muzny, D. M., Wheeler, D. A., Willerson, J. T., Yu, R. K., Shete, S. S., Scherer, S. E., Raman, C. S., Buja, L. M. and Milewicz, D. M. (2009). Mutations in smooth muscle alpha-actin (acta2) cause coronary artery disease, stroke and moyamoya disease, along with thoracic aortic disease. *Am. J. Hum. Genet*. **84**, 617-627.

Hahn, C. and Schwartz, M. A. (2009). Mechanotransduction in vascular physiology and atherogenesis. *Nat. Rev. Mol. Cell Biol*. **10**, 53-62.

Halka, A. T., Turner, N. J., Carter, A., Ghosh, J., Murphy, M. O., Kirton, J. P., Kielty, C. M. and Walker, M. G. (2008). The effects of stretch on vascular smooth muscle cell phenotype in vitro. *Cardiovasc. Pathol*. **17**, 98-102.

Han, R., Li, Z., Fan, Y., and Jiang, Y. (2013). Recent advances in super-resolution fluorescence imaging and its applications in biology. *J. Genet. Genomics*. **40**, 583-595.

Hayashi, K. and Naiki, T. (2009). Adaptation and remodeling of vascular wall; biomechanical response to hypertension. *J. Mech. Behav. Biomed. Mater.* **2**, 3-19.

Heinrichs, A. 2009. Mechanotransduction: switch and stretch. *Nat. Rev. Mol. Cell Biol*. **10**, 163-163.

Herrmann, H., Strelkov, S. V., Burkhard, P. and Aebi, U. (2009). Intermediate filaments: primary determinants of cell architecture and plasticity. *J. Clin. Invest*. **119**, 1772-1783.

Hertz, H. (1881). Ueber die beruhrung fester elastischer korper. *Journal für die reine und angewandte Mathematik.* **92**, 156-171.

Hibbs, A. R. (2004). Confocal microscopy for biologists. New York, NY: Kluwer Academic/Plenum Publishers.

Hirschfeld, T. (1965). Total reflection fluorescence. *Can. Spectrosc.* **10**, 128.

Hoffman, B. D., Grashoff, C. and Schwartz, M. A. (2011). Dynamic molecular processes mediate cellular mechanotransduction. *Nature*. **475**, 316-323.

Hong, F., Haldeman, B. D., Jackson, D., Carter, M., Baker, J. E. and Cremo, C. R. (2011). Biochemistry of smooth muscle myosin light chain kinase. *Arch. Biochem. Biophys*. **510**, 135-146.

Hooke, R. (1665). Micrographia, or, some physiological descriptions of minute bodies made by magnifying glasses, With observations and inquiries thereupon /by r. Hooke. Printed by Jo. Martyn and Ja. Allestry, printers to the Royal Society London.

Humphrey, J. D., Eberth, J. F., Dye, W. W. and Gleason, R. L. (2009). Fundamental role of axial stress in compensatory adaptations by arteries. *J. Biomech*. **42**, 1-8.

Hutter, J. L. and Bechhoefer, J. (1993). Calibration of atomic-force microscope tips. *Rev. Sci. Instr*. **64**, 1868-1873.

Huveneers, S. and Danen, E. H. (2009). Adhesion signaling - crosstalk between integrins, Src and Rho. *J. Cell Sci*. **122**, 1059-1069.

Huveneers, S., Truong, H., Fassler, R., Sonnenberg, A. and Danen, E. H. (2008). Binding of soluble fibronectin to integrin alpha5 beta1 - link to focal adhesion redistribution and contractile shape. *J. Cell Sci*. **121**, 2452-2462.

Huveneers, S., van den Bout, I., Sonneveld, P., Sancho, A., Sonnenberg, A. and

Danen, E. H. (2007). Integrin alpha v beta 3 controls activity and oncogenic potential of primed c-Src. *Cancer Res*. **67**, 2693-2700.

Hynes, R. O. (2002). Integrins: bidirectional, allosteric signaling machines. *Cell*. **110**, 673-687.

Ingber, D.E. (1998). The architecture of life. *Sci Am*. **278**,48-57.

Ingber, D. E. (2002). Mechanical signaling and the cellular response to extracellular matrix in angiogenesis and cardiovascular physiology. *Circ. Res*. **91**, 877-887.

Ingber, D. E. (2006). Cellular mechanotransduction: putting all the pieces together again. *FASEB J*. **20**, 811-827.

Inoué, S. and Inoué, T. (2002). Chapter 2 - direct-view high-speed confocal scanner, The CSU-10. In: *Methods in Cell Biology, Vol. 70* (ed M. Brian), pp. 87-127. San Diego, CA: Academic Press.

Intengan, H. D. and Schiffrin, E. L. (2000). Structure and mechanical properties of resistance arteries in hypertension: role of adhesion molecules and extracellular matrix determinants. *Hypertension*. **36**, 312-318.

Jaalouk, D. E. and Lammerding, J. (2009). Mechanotransduction gone awry. *Nat. Rev. Mol. Cell. Biol*. **10**, 63-73.

Janssen, L .J., Lu-Chao, H. and Netherton, S. (2001). Excitation-contraction coupling in pulmonary vascular smooth muscle involves tyrosine kinase and Rho kinase. *Am. J. Physiol. Lung Cell Mol. Physiol*. **280**, L666-L674.

Jiang, G., Huang, A. H., Cai, Y., Tanase, M. and Sheetz, M. P. (2006). Rigidity sensing at the leading edge through alphavbeta3 integrins and RPTPalpha. *Biophys J*. **90**, 1804-1809.

Kanchanawong, P., Shtengel, G., Pasapera, A. M., Ramko, E. B., Davidson, M. W., Hess, H. F. and Waterman, C. M. (2010). Nanoscale architecture of integrin-based cell adhesions. *Nature*. **468**, 580-584.

Kaplan, K. B., Bibbins, K. B., Swedlow, J. R., Arnaud, M., Morgan, D. O. and Varmus, H. E. (1994). Association of the amino-terminal half of c-Src with focal adhesions alters their properties and is regulated by phosphorylation of tyrosine 527. *EMBO J*. **13**, 4745-4756.

Kaplan, K. B., Swedlow, J. R., Morgan, D. O. and Varmus, H. E. (1995). C-Src enhances the spreading of Src-/- fibroblasts on fibronectin by a kinase-independent mechanism. *Genes Dev*. **9**, 1505-1517.

Katoh, K., Kano, Y., Amano, M., Kaibuchi, K. and Fujiwara, K. (2001). Stress fiber organization regulated by MLCK and Rho-kinase in cultured human fibroblasts. *Am. J. Physiol. Cell Physiol*. **280**, C1669-C1679.

Kaunas, R. and Deguchi, S. (2011). Multiple roles for myosin II in tensional homeostasis under mechanical loading. *Cell. Molec. Bioeng*. **4**, 182-191.

Kim, H. R., Gallant, C., Leavis, P. C., Gunst, S. J. and Morgan, K. G. (2008). Cytoskeletal remodeling in differentiated vascular smooth muscle is actin isoform dependent and stimulus dependent. *Am. J. Physiol. Cell Physiol*. **295**,

C768-C778.

Kino, G. S. (1995). Intermediate optics in nipkow disk microscopes. In: *Handbook of Biological Confocal Microscopy,* (ed J. Pawley). pp. 155-165. United States: Springer.

Kirchner, J., Kam, Z., Tzur, G., Bershadsky, A. D. and Geiger, B. (2003). Live-cell monitoring of tyrosine phosphorylation in focal adhesions following microtubule disruption. *J. Cell Sci*. **116**, 975-986.

Kjoller, L. and Hall, A. (1999). Signaling to Rho GTPases. *Exp. Cell Res*. **253**, 166-179.

Knock, G. A., Snetkov, V. A., Shaifta, Y., Drndarski, S., Ward, J. P. and Aaronson, P. I. (2008). Role of Src-family kinases in hypoxic vasoconstriction of rat pulmonary artery. *Cardiovasc. Res*. **80**, 453-462.

Kong, F., Garcia, A. J., Mould, A. P., Humphries, M. J. and Zhu, C. (2009). Demonstration of catch bonds between an integrin and its ligand. *J. Cell Biol*. **185**, 1275-1284.

Kumar, A. and Lindner, V. (1997). Remodeling with neointima formation in the mouse carotid artery after cessation of blood flow. *Arterioscler. Thromb. Vasc. Biol*. **17**, 2238-2244.

Kureishi, Y., Kobayashi, S., Amano, M., Kimura, K., Kanaide, H., Nakano, T., Kaibuchi, K. and Ito, M. (1997). Rho-associated kinase directly induces smooth muscle contraction through myosin light chain phosphorylation. *J. Biol. Chem*.

272, 12257-12260.

Lal, R. and John, S. A. (1994). Biological applications of atomic force microscopy. *Am. J. Physiol*. **266**, C1-C21.

Lansbergen, G. and Akhmanova, A. (2006). Microtubule plus end: a hub of cellular activities. *Traffic*. **7**, 499-507.

Lee, K.-M., Tsai, K. Y., Wang, N. and Ingber, D. E. (1998). Extracellular matrix and pulmonary hypertension: control of vascular smooth muscle cell contractility. *Am. J. Physiol.* 274, H76-H82.

Lettau, M., Pieper, J. and Janssen, O. (2009). Nck adapter proteins: functional versatility in t cells. *Cell Commun. Signal*. **7**, 1.

Li, C. and Xu, Q. (2000). Mechanical stress-initiated signal transductions in vascular smooth muscle cells. *Cell Signal*. **12**, 435-445.

Lim, S. M., Kreipe, B. A., Trzeciakowski, J., Dangott, L. and Trache, A. (2010). Extracellular matrix effect on rhoa signaling modulation in vascular smooth muscle cells. *Exp. Cell Res*. **316**, 2833-2848.

Lim, S. M., Trzeciakowski, J. P., Sreenivasappa, H., Dangott, L. J. and Trache, A. (2012). Rhoa-induced cytoskeletal tension controls adaptive cellular remodeling to mechanical signaling. *Integr. Biol. (Camb)*. **4**, 615-627.

Loirand, G. and Pacaud, P. (2010). The role of rho protein signaling in hypertension. *Nat. Rev. Cardiol*. **7**, 637-647.

Mack, C. P., Somlyo, A. V., Hautmann, M., Somlyo, A. P. and Owens, G. K. (2001). Smooth muscle differentiation marker gene expression is regulated by Rhoa-mediated actin polymerization. *J. Biol. Chem*. **276**, 341-347.

Maekawa, M., Ishizaki, T., Boku, S., Watanabe, N., Fujita, A., Iwamatsu, A., Obinata, T., Ohashi, K., Mizuno, K. and Narumiya, S. (1999). Signaling from rho to the actin cytoskeleton through protein kinases rock and lim-kinase. *Science*. **285**, 895-898.

Majesky, M. W. 2007. Developmental basis of vascular smooth muscle diversity. *Arterioscler. Thromb. Vasc. Biol*. **27**, 1248-1258.

Marshall, B. T., Long, M., Piper, J. W., Yago, T., McEver, R. P. and Zhu, C. (2003). Direct observation of catch bonds involving cell-adhesion molecules. *Nature*. **423**, 190-193.

Martinez-Lemus, L. A., Crow, T., Davis, M. J. and Meininger, G. A. (2004). Alpha(5)beta(1) and alpha(v)beta(3) integrins are required for myogenic constriction of arterioles. *Cardiovasc. Pathol*. **13**, 191.

Martinez-Lemus, L. A., Sun, Z., Trache, A., Trzciakowski, J. P. and Meininger, G. A. (2005). Integrins and regulation of the microcirculation: From arterioles to molecular studies using atomic force microscopy. *Microcirculation*. **12**, 99-112.

Martinez-Lemus, L. A., Hill, M. A. and Meininger, G. A. (2009). The plastic nature of the vascular wall: a continuum of remodeling events contributing to control of arteriolar diameter and structure. *Physiology (Bethesda)*. **24**, 45-57.

Martinez-Lemus, L. A., Wu, X., Wilson, E., Hill, M. A., Davis, G. E., Davis, M. J. and Meininger, G. A. (2003). Integrins as unique receptors for vascular control. *J. Vasc. Res*. 40, 211-233.

Matthews, B. D., Overby, D. R., Mannix, R. and Ingber, D. E. (2006). Cellular adaptation to mechanical stress: role of integrins, Rho, cytoskeletal tension and mechanosensitive ion channels. *J. Cell Sci*. **119**, 508-518.

Milewicz, D. M., Ostergaard, J. R., Ala-Kokko, L. M., Khan, N., Grange, D. K., Mendoza-Londono, R., Bradley, T. J., Olney, A. H., Ades, L., Maher, J. F., Guo, D., Buja, L. M., Kim, D., Hyland, J. C. and Regalado, E. S. (2010). De novo acta2 mutation causes a novel syndrome of multisystemic smooth muscle dysfunction. *Am. J. Med. Genet. A*. **152A**, 2437-2443.

Mogford, J. E., Davis, G. E. and Meininger, G. A. (1997). RGDN peptide interaction with endothelial alpha5beta1 integrin causes sustained endothelin-dependent vasoconstriction of rat skeletal muscle arterioles. *J. Clin. Invest*. **100**, 1647-1653.

Moolenaar, W. H. (1995). Lysophosphatidic acid signalling. *Curr. Opin. Cell Biol*. **7**, 203-210.

Morgan, M. R., Humphries, M. J. and Bass, M. D. (2007). Synergistic control of cell adhesion by integrins and syndecans. *Nat. Rev. Mol. Cell Biol*. **8**, 957-969.

Morris, V. J., Kirby, A. R. and Gunning, A. P. (1999). Atomic force microscopy for biologists. London, UK: Imperial College Press.

Muggeo, V. M. (2003). Estimating regression models with unknown break-points. *Stat.*

Med. **22**, 3055-3071.

Murphy, R. A. (1994). What is special about smooth muscle? The significance of covalent crossbridge regulation. *FASEB J*. **8**, 311-318.

Nakao, F., Kobayashi, S., Mogami, K., Mizukami, Y., Shirao, S., Miwa, S., Todoroki-Ikeda, N., Ito, M. and Matsuzaki, M. (2002). Involvement of Src family protein tyrosine kinases in Ca(2+) sensitization of coronary artery contraction mediated by a sphingosylphosphorylcholine-Rho-kinase pathway. *Circ. Res*. **91**, 953-960.

Narumiya, S., Ishizaki, T. and Uehata, M. (2000). Use and properties of rock-specific inhibitor y-27632. *Methods Enzymol*. **325**, 273-284.

Nienhaus, K. and Ulrich Nienhaus, G. (2014). Fluorescent proteins for live-cell imaging with super-resolution. *Chem. Soc. Rev*. **43**, 1088-1106.

Nunes, K. P., Rigsby, C. S. and Webb, R. C. (2010). Rhoa/rho-kinase and vascular diseases: what is the link? *Cell. Mol. Life Sci*. **67**, 3823-3836.

Ohanian, J., Ohanian, V., Shaw, L., Bruce, C. and Heagerty, A. M. (1997). Involvement of tyrosine phosphorylation in endothelin-1-induced calcium-sensitization in rat small mesenteric arteries. *Br. J. Pharmacol*. **120**, 653-61.

Ohata, H., Aizawa, H. and Momose, K. (1997). Lysophosphatidic acid sensitizes mechanical stress-induced Ca2+ response via activation of phospholipase c and tyrosine kinase in cultured smooth muscle cells. *Life Sci*. **60**, 1287-1295.

Orr, A. W., Helmke, B. P., Blackman, B. R. and Schwartz, M. A. (2006). Mechanisms of mechanotransduction. *Dev. Cell*. **10**, 11-20.

Owens, G. K. (1995). Regulation of differentiation of vascular smooth muscle cells. *Physiol. Rev*. **75**, 487-517.

Papke, C. L., Cao, J., Kwartler, C. S., Villamizar, C., Byanova, K. L., Lim, S. M., Sreenivasappa, H., Fischer, G., Pham, J., Rees, M., Wang, M., Chaponnier, C., Gabbiani, G., Khakoo, A. Y., Chandra, J., Trache, A., Zimmer, W. and Milewicz, D. M. (2013). Smooth muscle hyperplasia due to loss of smooth muscle α-actin is driven by activation of focal adhesion kinase, altered p53 localization and increased levels of platelet-derived growth factor receptor-β. *Hum. Mol. Genet*. **22**, 3123-3137.

Parsons, J. T., Horwitz, A. R. and Schwartz, M. A. (2010). Cell adhesion: integrating cytoskeletal dynamics and cellular tension. *Nat. Rev. Mol. Cell Biol*. **11**, 633-643.

Pawley, J. B. (2006). Appendix 3: "More than you ever really wanted to know about charge-coupled devices". In: *Handbook of Biological Confocal Microscopy (3rd Ed.)*. United States: Springer Science+Business Media.

Petit, V. and Thiery, J. P. (2000). Focal adhesions: structure and dynamics. *Biol. Cell*. **92**, 477-494.

Petrie, R. J., Doyle, A. D. and Yamada, K. M. (2009). Random versus directionally persistent cell migration. *Nat. Rev. Mol. Cell Biol*. **10**, 538-549.

Pistea, A., Bakker, E. N., Spaan, J. A. and VanBavel, E. (2005). Flow inhibits inward

remodeling in cannulated porcine small coronary arteries. *Am. J. Physiol. Heart Circ. Physiol*. **289**, H2632-H2640.

Pries, A. R., Reglin, B. and Secomb, T. W. (2005). Remodeling of blood vessels: responses of diameter and wall thickness to hemodynamic and metabolic stimuli. *Hypertension*. **46**, 725-731.

Pries, A. R. and Secomb, T. W. (2002). Structural adaptation of microvascular networks and development of hypertension. *Microcirculation*. **9**, 305-14.

Putman, C. A., van der Werf, K. O., de Grooth, B. G., van Hulst, N. F. and Greve, J. (1994). Viscoelasticity of living cells allows high resolution imaging by tapping mode atomic force microscopy. *Biophys. J*. **67**, 1749-1753.

Radmacher, M., Tillamnn, R. W., Fritz, M. and Gaub, H. E. (1992). From molecules to cells: Imaging soft samples with the atomic force microscope. *Science*. **257**, 1900-1905.

Rasband, W. S. (1997-2004). Imagej. Bethesda, MD: National Institutes of Health.

Ridley, A. J. and Hall, A. (1992). The small GTP-binding protein rho regulates the assembly of focal adhesions and actin stress fibers in response to growth factors. *Cell*. **70**, 389-399.

Rolfe, B. E., Worth, N. F., World, C. J., Campbell, J. H. and Campbell, G. R. (2005). Rho and vascular disease. *Atherosclerosis*. **183**, 1-16.

Romer, L. H., Birukov, K. G. and Garcia, J. G. (2006). Focal adhesions: paradigm for

a signaling nexus. *Circ. Res*. **98**, 606-16.

Ruoslahti, E. (1996). RGD and other recognition sequences for integrins. *Annu Rev. Cell Dev. Biol*. **12**, 697-715.

Saga, H., Kimura, K., Hayashi, K., Gotow, T., Uchiyama, Y., Momiyama, T., Tadokoro, S., Kawashima, N., Jimbou, A. and Sobue, K. (1999). Phenotype-dependent expression of alpha-smooth muscle actin in visceral smooth muscle cells. *Exp. Cell Res*. **247**, 279-92.

Sastry, S. K. and Burridge, K. (2000). Focal adhesions: a nexus for intracellular signaling and cytoskeletal dynamics. *Exp. Cell Res*. **261**, 25-36.

Schildmeyer, L. A., Braun, R., Taffet, G., Debiasi, M., Burns, A. E., Bradley, A. and Schwartz, R. J. (2000). Impaired vascular contractility and blood pressure homeostasis in the smooth muscle alpha-actin null mouse. *FASEB J.* **14**, 2213-2220.

Schwartz, M. A. and Shattil, S. J. (2000). Signaling networks linking integrins and rho family GTPases. *Trends Biochem. Sci*. **25**, 388-391.

Schwartz, S., Virmani, R. and Rosenfeld, M. (2000). The good smooth muscle cells in atherosclerosis. *Curr. Atheroscler. Rep*. **2**, 422-429.

Shadwick, R. E. (1999). Mechanical design in arteries. *J. Exp. Biol*. **202**, 3305-3313.

Sharf, Y., Seo, Y., Eliav, U., Akselrod, S. and Navon, G. (1998). Mapping strain exerted on blood vessel walls using deuterium double-quantum-filtered MRI.

Proc. Natl. Acad. Sci. U S A. **95**, 4108-4112.

Shynlova, O., Tsui, P., Dorogin, A., Chow, M. and Lye, S. J. (2005). Expression and localization of alpha-smooth muscle and gamma-actins in the pregnant rat myometrium. *Biol. Reprod*. **73**, 773-780.

Silverman, B. W. (1986). Density estimation for statistics and data analysis. Boca Raton, FL: CRC Press.

Small, J. V. and North, A. J. (1995). Architecture of the smooth muscle cell. In: *Vascular Smooth Muscle Cell* (ed. S. M. Schwartz and R. P. Machem), pp. 169–185. San Diego, CA: Academic Press.

Sneddon, I. N. (1965). The relation between load and penetration in the axisymmetric boussinesq problem for a punch of arbitrary profile. *Intl. J. Eng. Sci*. **3**, 47-57.

Sreenivasappa, H., Chaki, S. P., Lim, S. M., Trzeciakowski, J. P., Davidson, M. W., Rivera, G. M. and Trache, A. (2014). Selective regulation of cytoskeletal tension and cell-matrix adhesion by RhoA and Src. *Integr. Biol. (Camb)*. **6**, 743-754.

Srichai, M. B. and Zent, R. (2010). Integrin structure and function. In: *Cell-Extracellular Matrix Interactions in Cancer* (ed. R. Zent and A. Pozzi), pp. 19–41. New York, NY: Springer Science+Business Media.

Stary, H. C., Chandler, A. B., Dinsmore, R. E., Fuster, V., Glagov, S., Insull, W., Jr., Rosenfeld, M. E., Schwartz, C. J., Wagner, W. D. and Wissler, R. W. (1995). A definition of advanced types of atherosclerotic lesions and a

histological classification of atherosclerosis. A report from the Committee on Vascular Lesions of the Council on Arteriosclerosis, American Heart Association. *Arterioscler. Thromb. Vasc. Biol*. **15**, 1512-1531.

Stehbens, W. E. and Martin, B. J. (1993). Ultrastructural alterations of collagen fibrils in blood vessel walls. *Connect Tissue Res*. **29**, 319-331.

Subauste, M. C., Von Herrath, M., Benard, V., Chamberlain, C. E., Chuang, T. H., Chu, K., Bokoch, G. M. and Hahn, K. M. (2000). Rho family proteins modulate rapid apoptosis induced by cytotoxic t lymphocytes and fas. *J. Biol. Chem*. **275**, 9725-9733.

Sugita, S., Adachi, T., Ueki, Y. and Sato, M. (2011). A novel method for measuring tension generated in stress fibers by applying external forces. *Biophys J*. **101**, 53-60.

Sun, Z., Huang, S., Li, Z. and Meininger, G. A. (2012). Zyxin is involved in regulation of mechanotransduction in arteriole smooth muscle cells. *Front. Physiol*. **3**, 472.

Sun, Z., Martinez-Lemus, L. A., Hill, M. A. and Meininger, G. A. (2008). Extracellular matrix-specific focal adhesions in vascular smooth muscle produce mechanically active adhesion sites. *Am. J. Physiol. Cell Physiol*. **295**, C268-C278.

Sun, Z., Martinez-Lemus, L. A., Trache, A., Trzeciakowski, J. P., Davis, G. E., Pohl, U. and Meininger, G. A. (2005). Mechanical properties of the interaction

between fibronectin and alpha5beta1-integrin on vascular smooth muscle cells studied using atomic force microscopy. *Am. J. Physiol. Heart. Circ. Physiol*. **289**, H2526-H2535.

Tadokoro, S., Shattil, S. J., Eto, K., Tai, V., Liddington, R. C., de Pereda, J. M., Ginsberg, M. H. and Calderwood, D. A. (2003). Talin binding to integrin β tails: a final common step in integrin activation. *Science*. **302**, 103-106.

Takagi, J., Petre, B. M., Walz, T. and Springer, T. A. (2002). Global conformational rearrangements in integrin extracellular domains in outside-in and inside-out signaling. *Cell*. **110**, 599-611.

Takeji, M., Moriyama, T., Oseto, S., Kawada, N., Hori, M., Imai, E. and Miwa, T. (2006). Smooth muscle alpha-actin deficiency in myofibroblasts leads to enhanced renal tissue fibrosis. *J. Biol. Chem*. **281**, 40193-40200.

Thomas, W. E., Vogel, V. and Sokurenko, E. (2008). Biophysics of catch bonds. *Annu. Rev. Biophys*. **37**, 399-416.

Trache, A. and Lim, S. M. (2009). Integrated microscopy for real-time imaging of mechanotransduction studies in live cells. *J. Biomed. Opt*. **14**, 034024.

Trache, A. and Lim, S. M. (2010). Live cell response to mechanical stimulation studied by integrated optical and atomic force microscopy. *J. Vis Exp*. **pii**, 2072

Trache, A. and Meininger, G. A. (2008a). Atomic force microscopy (AFM). *Curr. Protoc. Microbiol*. Chapter 2, Unit 2C 2.

Trache, A. and Meininger, G. A. (2008b). Total internal reflection fluorescence (TIRF) microscopy. *Curr. Protoc. Microbiol*. Chapter 2, Unit 2A 2 1-2A 2 22.

Trache, A., Trzeciakowski, J. P., Gardiner, L., Sun, Z., Muthuchamy, M., Guo, M., Yuan, S. Y. and Meininger, G. A. (2005). Histamine effects on endothelial cell fibronectin interaction studied by atomic force microscopy. *Biophys. J*. **89**, 2888-2898.

Trzeciakowski, J. P. and Meininger, G. A. (2004). NForceR*:* nanoscale force reader and AFM data analysis package.

Turner, C. E., Kramarcy, N., Sealock, R. and Burridge, K. (1991). Localization of paxillin, a focal adhesion protein, to smooth muscle dense plaques and the myotendinous and neuromuscular junctions of skeletal muscle. *Exp. Cell Res*. **192**, 651-655.

Tyler, W. J. (2012). The mechanobiology of brain function. *Nat. Rev. Neurosci*. **13**, 867-878.

Van Eyk, J. E., Arrell, D. K., Foster, D. B., Strauss, J. D., Heinonen, T. Y., Furmaniak-Kazmierczak, E., Cote, G. P. and Mak, A. S. (1998). Different molecular mechanisms for Rho family GTPase-dependent, Ca^{2+}-independent contraction of smooth muscle. *J. Biol. Chem*. **273**, 23433-23439.

Van Vliet, K. J., Bao, G. and Suresh, S. (2003). The biomechanics toolbox: experimental approaches for living cells and biomolecules. *Acta Materialia*. **51**, 5881-5905.

VanBavel, E., Siersma, P. and Spaan, J. A. (2003). Elasticity of passive blood vessels: a new concept. *Am. J. Physiol. Heart Circ. Physiol*. **285**, H1986-H2000.

Vandekerckhove, J. and Weber, K. (1978). At least six different actins are expressed in a higher mammal: an analysis based on the amino acid sequence of the amino-terminal tryptic peptide. *J. Mol. Biol*. **126**, 783-802.

Venables, W. N. and Ripley, B. D. (1994). Modern applied statistics with s-plus. New York: Springer.

Volberg, T., Romer, L., Zamir, E. and Geiger, B. (2001). Pp60(c-src) and related tyrosine kinases: a role in the assembly and reorganization of matrix adhesions. *J. Cell Sci*. **114**, 2279-2289.

Wagenseil, J. E. and Mecham, R. P. (2009). Vascular extracellular matrix and arterial mechanics. *Physiol. Rev*. **89**, 957-989.

Wang, Y., Botvinick, E. L., Zhao, Y., Berns, M. W., Usami, S., Tsien, R. Y. and Chien, S. (2005). Visualizing the mechanical activation of src. *Nature*. **434**, 1040-1045.

Watanabe, N., Kato, T., Fujita, A., Ishizaki, T. and Narumiya, S. (1999). Cooperation between mdia1 and rock in rho-induced actin reorganization. *Nat. Cell Biol*. **1**, 136-143.

Weber, M. A., Neutel, J. M. and Cheung, D. G. (1989). Hypertension in the aged:a pathophysiologic basis for treatment. *Am. J. Cardiol*. **63**, 25H-32H.

Westerhof, N. and O'Rourke, M. F. (1995). Haemodynamic basis for the development of left ventricular failure in systolic hypertension and for its logical therapy. *J. Hypertens*. **13**, 943-952.

White, D. P., Caswell, P. T. and Norman, J. C. (2007). Alpha v beta3 and alpha5beta1 integrin recycling pathways dictate downstream rho kinase signaling to regulate persistent cell migration. *J. Cell Biol*. **177**, 515-525.

Wirth, A. (2010). Rho kinase and hypertension. *Biochim. Biophys. Acta*. **1802**, 1276-1284.

Wolfenson, H., Bershadsky, A., Henis, Y. I. and Geiger, B. (2011). Actomyosin-generated tension controls the molecular kinetics of focal adhesions. *J. Cell Sci*. **124**, 1425-1432.

Woodsome, T. P., Polzin, A., Kitazawa, K., Eto, M. and Kitazawa, T. (2006). Agonist- and depolarization-induced signals for myosin light chain phosphorylation and force generation of cultured vascular smooth muscle cells. *J. Cell Sci*. **119**, 1769-1780.

Worth, N. F., Campbell, G. R., Campbell, J. H. and Rolfe, B. E. (2004). Rho expression and activation in vascular smooth muscle cells. *Cell Motil Cytoskeleton*. **59**, 189-200.

Worth, N. F., Rolfe, B. E., Song, J. and Campbell, G. R. (2001). Vascular smooth muscle cell phenotypic modulation in culture is associated with reorganisation of contractile and cytoskeletal proteins. *Cell Motil. Cytoskeleton*. **49**, 130-145.

Wu, X., Mogford, J. E., Platts, S. H., Davis, G. E., Meininger, G. A., and Davis, M. J. (1998). Modulation of calcium current in arteriolar smooth muscle by alphav beta3 and alpha5 beta1 integrin ligands. *J. Cell Biol.* **143**, 241-52.

Wu, X., Davis, G. E., Meininger, G. A., Wilson, E. and Davis, M. J. (2001). Regulation of the l-type calcium channel by alpha 5beta 1 integrin requires signaling between focal adhesion proteins. *J. Biol. Chem*. **276**, 30285-30292.

You, H. and Yu, L. (1999). Atomic force microscopy imaging of living cells: progress, problems and prospects. *Methods Cell Sci*. **21**, 1-17.

Zaidel-Bar, R., Itzkovitz, S., Ma'ayan, A., Iyengar, R. and Geiger, B. (2007). Functional atlas of the integrin adhesome. *Nat. Cell Biol.* **9**, 858-867.

Zaidel-Bar, R. and Geiger, B. (2010). The switchable integrin adhesome. *J. Cell Sci.* **123**, 1385-1388

Zhang, W. and Gunst, S. J. (2006). Dynamic association between alpha-actinin and beta-integrin regulates contraction of canine tracheal smooth muscle. *J. Physiol*. **572**, 659-676.

Zhou, Q. and Liao, J. K. (2009). Rho kinase: an important mediator of atherosclerosis and vascular disease. *Curr. Pharm. Des*. **15**, 3108-3115.